Journal of Hydrology 594 (2021) 125778

Contents lists available at ScienceDirect

Journal of Hydrology

journal homepage: www.elsevier.com/locate/jhydrol

Research papers

Geochemical mechanisms of natural arsenic mobility in the hydrogeologic system of Lower Katari Basin, Bolivian Altiplano

Israel Quino Lima [a,b,*], Oswaldo Eduardo Ramos Ramos [a], Mauricio Ormachea Muñoz [a], Maria Isabel Chambi Tapia [a], Jorge Quintanilla Aguirre [a], Arslan Ahmad [b,c,d,e], Jyoti Prakash Maity [f], Md. Tahmidul Islam [b], Prosun Bhattacharya [b,c,*]

[a] Laboratorio de Hidroquímica, Instituto de Investigaciones Químicas, Universidad Mayor de San Andrés, La Paz, Bolivia
[b] KTH-International Groundwater Arsenic Research Group, Department of Sustainable Development, Environmental Science and Engineering, KTH Royal Institute of Technology, Teknikringen 10B, SE-10044 Stockholm, Sweden
[c] KWR Water Cycle Research Institute, Groningenhaven 7, 3433 PE Nieuwegein, the Netherlands
[d] Department of Environmental Technology, Wageningen University and Research (WUR), Droevendaalsesteeg 4, 6708 PB Wageningen, the Netherlands
[e] SIBELCO Ankerpoort NV, Op de Bos 300, 6223 EP Maastricht, the Netherlands
[f] Department of Earth and Environmental Sciences, National Chung Cheng University, 168 University Road, Min-Hsiung, Chiayi County 62102, Taiwan

ARTICLE INFO

This manuscript was handled by Huaming Guo, Editor-in-Chief

Keywords:
Arsenic Bolivian Altiplano
Geochemistry
Groundwater
Spatio-temporal Variation
Hydrogeology
Katari River

ABSTRACT

Arsenic (As) contamination of drinking water is a worldwide problem. The natural origin of As, its mobility, and transport are of paramount interest in Bolivian Altiplano due to its presence in mineral deposits, brines, hot springs, and volcanic rocks. In this study, a geochemical spatial–temporal approach was used to understand the sources and factors that regulate the mobilization and fate of As in water bodies as well as sediments of Lower Katari Basin (LKB). The study reveals that high levels of As (288 μg/L), boron (B) (2473 μg/L), manganese (Mn) (7259 μg/L), and high salinity (23850 μS/cm) are present in shallow drinking water wells, which exceed the guideline values of the Bolivian regulation (NB-512) and WHO. Seasonal changes (mean monthly rainfall in the dry and rainy period: 6–89 mm) and their impact on water quantity (0.9–5.1 m^3/s), in addition to the load of solids and liquids of residual origin (Pallina River), pose health risks for the communities at the banks of the Katari River. The hydrogeological study indicates that the groundwater flows from southeast to northwest (SE–NW), which indicate interaction between groundwater and surface water in this region. The spatial distribution of As varies considerably due to geological characteristics of the area as well as due to the heterogeneously distributed evaporites in the sediments (alluvial, fluvial-lacustrine); however, the highest concentrations of As are observed in the alluvial sediments of the northern region. Sequential extraction (BCR) of sediments along with geochemical modeling (mineral saturation indices) indicates that iron (Fe) and aluminum (Al) (hydr)oxides are the most important adsorbent minerals of As in the central and southern region of LKB. The hydrochemistry of water bodies in LKB is strongly influenced by the interaction with the sediment constituents and by the spatial–temporal variations. Therefore, the determination of the distribution of As among the different geochemical fractions was useful to find the relative proportions of As transported by different chemical mechanisms (adsorption/dissolution) and their spatial–temporal variation.

Abbreviations: TEs, Trace Elements; GW, Groundwater; SW, Surface Water; EC, Electrical Conductivity; TDS, Total Dissolved Solid; DO, Dissolved Oxygen; OC, Organic Carbon; Eh, redox potential; LKB, Lower Katari Basin; CB, Cohana Bay; BP, Before the Present; TDPS, Lake Titicaca, Desaguadero River, Poopó River, Salt Flat of Coipasa; CBE, Charge Balance Error; bdl, Below detection limit; NB-512, Norma Boliviana – 512 [National regulation for the control of water quality for human consumption]; WHO, World Health Organization; SI, Saturation Indices; BCR, Community Bureau of Reference; CS, Core Sediments; RS, River Sediments; ITCZ, Inter Tropical Convergence Zone; RASE, Rainy Seasons; DRSE, Dry Season; FEB16GW, February 2016 Groundwater; MAR17GW, March 2017 Groundwater; OCT16GW, October 2016 Groundwater; AUG17GW, August 2017 Groundwater; FEB16SW, February 2016 Surface Water; MAR17SW, March 2017 Surface Water; OCT16SW, October 2016 Surface Water; AUG17SW, August 2017 Surface Water; GIS, Geographic Information Systems; GIC, Geometrical Interval Classification; F1, Exchangeable Fraction; F2, Reducible Fraction; F3, Oxidizable Fraction; F4, Residual Fraction.

* Corresponding authors at: KTH-International Groundwater Arsenic Research Group, Department of Sustainable Development, Environmental Science and Engineering, KTH Royal Institute of Technology, Stockholm, Sweden.
E-mail addresses: israelql@kth.se (I. Quino Lima), prosun@kth.se (P. Bhattacharya).

https://doi.org/10.1016/j.jhydrol.2020.125778
Received 3 June 2020; Received in revised form 12 November 2020; Accepted 14 November 2020
Available online 6 December 2020

1. Introduction

Around the world, the presence of geogenic arsenic (As) in drinking water can cause human health problems such as skin pigmentation, palmar and plantar hyperkeratoses, gastrointestinal symptoms, anemia, various skin cancers, and liver disease (Hall, 2002; Kapaj et al., 2006; Nriagu et al., 2007; Maity et al., 2012). An estimated 150 million people are affected by As contamination in the world, and this number increases as new cases are discovered (Ravenscroft et al., 2009). Arsenic concentrations in groundwater (GW), exceeding the WHO guideline (10 μg/L), are well-known in several countries in the world (e.g. Spain, Portugal, Iran, China, and Hungary), particularly in the south and southeast Asia such as India, Bangladesh, and Vietnam (Bhattacharya et al., 1997, 2002a, 2002b, 2007, 2011; Maity et al., 2019, 2017, 2012, 2011a, 2011b; Smedley and Kinniburgh, 2002; Mukherjee et al., 2009, 2011; Jia et al., 2014; Bundschuh et al., 2012; Islam et al., 2013; Samal et al., 2013; Hamidian et al., 2019; Sohrabi et al., 2020), and in Latin America such as Mexico, Nicaragua, Ecuador, Chile, Argentina, Peru, Brazil and Uruguay (Bundschuh et al., 2008, 2009, 2010, 2012, 2020; Mukherjee et al., 2014; Raychowdhury et al., 2014; Litter et al., 2019a, 2019b; Tapia et al., 2019, 2020; Aullón Alcaine et al., 2020; Mariño et al., 2020; Mukherjee et al., 2020). Recent studies even indicate that As concentrations much lower than the WHO guideline can adversely affect human health and therefore countries like the Netherlands are optimizing their water treatment plants to produce drinking water with less than 1 μg/L As (Ahmad and Bhattacharya, 2019; Ahmad et al, 2020).

The spatio-temporal variation of As concentrations in GW could be the result of natural or anthropogenic factors (Avila Sandoval et al., 2018). In the case of natural variation in As concentrations, it could be a consequence of climatic and seasonal changes (wet and dry periods), although these factors are not commonly related to variation in As concentrations (Avila Sandoval et al., 2018; Ayotte et al., 2015).

The temporal variability of As concentrations in drinking water is a potential concern for human health studies (Ayotte et al., 2015). A fundamental aspect of the study of As contamination is that the degree to which the temporal variability of this analyte occurs in GW has not been well characterized. Many studies indicate that the As concentration in many aquifers is not particularly variable; However, other studies in lesser quantity reveal significant fluctuations over time (during periods of weeks to years) (Ayotte et al., 2015).

Arsenic concentrations in waters and sediments can normally be cumulatively high, due to the result of biogeochemical processes and anthropogenic activities. For this reason, the high concentrations of As in the sediments are of great environmental concern, since this analyte can be released into pore water and the overlying water by desorption and resuspension (Qin et al., 2014). The release and immobilization of As in the environment are fundamentally associated with factors such as pH, DO (dissolved oxygen), Eh, and other elements, in turn, microorganisms also play an important role in controlling the mobility of As in the environment (Qin et al., 2014; Ahmad et al., 2020).

A limited number of studies have so far been conducted on the occurrence and natural distribution of As in the Bolivian Altiplano (Quino et al., 2019; Quino Lima et al., 2020a, 2020b; Coomar et al., 2019; Tapia et al., 2020). High concentrations of As were reported in the samples of drinking water collected in an area not affected by mining, located in the south and west of the Lake Poopó Basin (Fig. 1) (PPO, 1996a; Hermansson and Karlsson, 2004; Van Den Bergh et al., 2010; Ramos Ramos et al., 2012; Ormachea Muñoz et al., 2013, 2016; Tapia and Audry, 2013; Tapia et al., 2020). In Lower Katari Basin (LKB) (Fig. 1), previous studies (IIS, 2013; Espinoza et al., 2016; Quino et al., 2019; Quino Lima et al., 2020a, 2020b) reported an elevated As concentrations in GW. The sources of As are present in different geological formations of the Bolivian Altiplano and multiple geochemical processes such as the weathering of volcanic rocks, adsorption–desorption of As from different sediments and the oxidation of sulfide minerals rich in As (Ormachea Muñoz et al., 2013; Coomar et al., 2019; Quino et al., 2019; Quino Lima et al., 2020a, 2020b) allow mobilization of As from rocks and sediments to surface water (SW) and GW (Tapia et al., 2012; Ramos Ramos et al., 2014).

The Katari Basin (including the LKB) and its tributaries (Seque, Seco, Pallina, and Katari rivers) as well as Cohana Bay (CB) (Fig. 2), are being highly affected due to the various water pollutants such as heavy metals, nutrient elements, and microbial contaminants. Some researchers (Chudnoff, 2006; Salvarredy-Aranguren et al., 2008; MMAyA, 2010; IIS, 2013; Duwig et al., 2014; Chiron and Duwig, 2016; Archundia et al., 2016, 2017; Quino et al., 2019) have carried out hydrological, physicochemical and microbiological investigations on water resources to understand the extent of this problem in the Katari Basin which includes the flood zones of the Seco, Seque, Pallina and Katari rivers, as well as the adjoining CB and impact on the population of the region.

The present research focuses on understanding (i) the geochemical characterization of As and other trace elements (TEs) in SW, GW, core sediments (CS), and river sediments (RS) in LKB, (ii) the natural distribution of As in LKB, (iii) the spatio-temporal variability of As and other TEs in GW and SW, and (iv) the hydrogeology of shallow GW in LKB.

2. Study area

2.1. General description of the study area

The TDPS (Lake Titicaca – Desaguadero River – Lake Poopó - Coipasa Salt Flat) system (Fig. 1) is a closed basin between Peruvian and Bolivian Altiplano with an area of 143,900 km^2 (ALT, 2017), comprising the watershed of Lake Titicaca (39%), Desaguadero River, Lake Poopó (38%) and Coipasa Salt Flat (23%) (CMPRALT, 2014). The TDPS system is located between Eastern and Western Cordillera from 3600 and 4500 m a.s.l. (OSRTOM, 1991). The maximum height is the Sajama mountain (6542 m a.s.l.), while the minimum height corresponds to the Coipasa

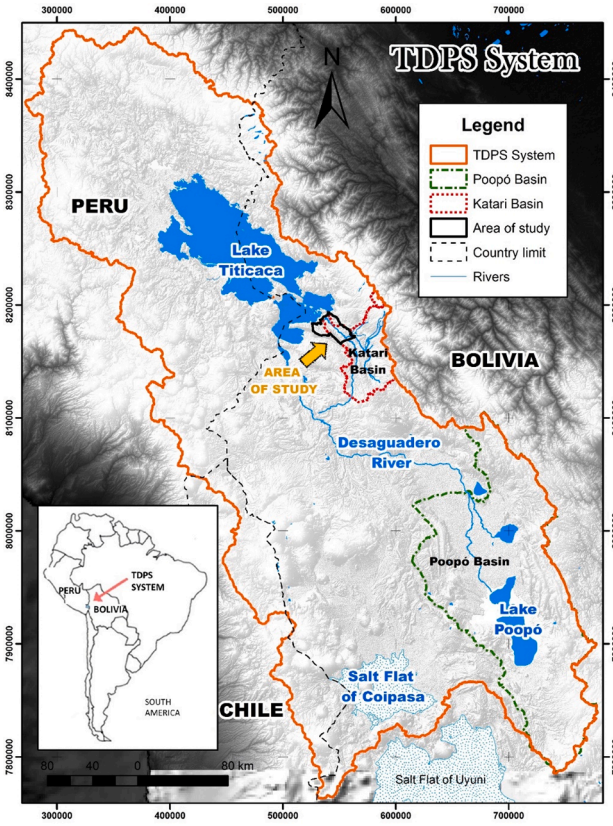

Fig. 1. Map of Lake Titicaca, Desaguadero River, Lake Poopó, and Coipasa Salt flat System (TDPS system), Katari Basin, and study area (Lower Katari Basin).

Salt Flat (3653 m a.s.l.) (CMPRALT, 2014).

The large depth (135 m mean depth) (ORSTOM, 1991; ALT, 2005), volume (903 km^3) (Pillco et al., 2019), high elevation (3,810 m a.s.l.) (Martínez et al., 2007) and its geographical location (tropical latitude) are characteristics that make the ecosystem generated by Lake Titicaca unique (Pillco et al., 2019). The sub-basins Katari, Coata, Huancané, Huaycho, Ilave, Illpa, Keka-Achacachi, Ramis, and Suchez are part of the Lake Titicaca Basin (Pillco et al., 2019; Martínez et al., 2007).

The Katari Basin (Fig. 1) has its origin in the Eastern Cordillera, where there are local mining activities (Milluni) (Fig. 2) (Archundia et al. 2017). Downstream, the Katari Basin encompasses the cities of El Alto and Viacha, which receives discharges from urban centers and many small-scale industries located along the banks of the Seque, Seco and Pallina rivers, tributaries of the Katari River (PNUMA, 2008, 2011; Ribera Arismendi, 2010; Archundia et al., 2017). Finally, the Katari Basin ends at CB, located on Lake Titicaca. The sub-basins such as Achicala, Anana Jahuira, Higher Katari, Lower Katari, Higher Pallina, Middle Pallina, Lower Pallina, Sallani, and Seque - Seco are part of the Katari Basin (MMAyA, 2010).

The study area is located in southeastern part of Lake Titicaca, with an elevation range between 3800 to 4200 m a.s.l., includes the entire LKB, part of Lower Pallina, Middle Pallina, Higher Katari, Sallani basins and part of CB (Fig. 2). It is part of four municipalities: Pucarani, Laja, Puerto Pérez and Tiahuanacu, has an area of >484 km^2 with 37,781 inhabitants distributed in rural communities of Quellani, Tircani, Queñapampa, Pujri, Machacamarca, Caycoma, Chacalleta, Iskacaspa, Masaya, Caleria, Huancarani, Mucuña, Caje, Catavi, Coachijo, Iquiaca, Korila, Quiripujo, Lacaya, Chojasivi, Huacullani, Wilajahuira, Aygachi, Cohana and Cascachi. El Alto and Viacha with >848,840 and 80,388 inhabitants (INE, 2017), respectively are the closest cities.

The inhabitants of these rural regions use GW from excavated and some drilled wells (mean: 4 m; range: 0.7–12.8 m), normally the wells are in dwellings, but a whole village uses others, in a few locations there are deep wells with pumps installed. In general, the water from these wells is dedicated to human consumption, but is also used for irrigation in a few locations.

2.2. Climate

In LKB, the climate is tempered with dry winter and soft summer, and is mainly determined by the seasonal movement of the Inter-Tropical Convergence Zone (ITCZ) and its high elevation (>3800 m a.s.l.) (MMAyA, 2010). The mean annual rainfall of the LKB is 509.86 mm, the rainiest months are December-January-February-March (mean monthly: 89.03 mm) and the driest months are May-June-July (mean monthly: 5.82 mm) (MMAyA, 2010). The mean annual temperature is 7.7 °C (Tiwanaku Station) and solar radiation (El Alto Station) has a high level of ultraviolet radiation (mean annual: 533 cal/cm^2/day), due to the low atmospheric density and a diaphanous atmosphere (IIS, 2013).

2.3. Geology

The study area is formed by scattered hills belonging to the Devonian period (sandstones, lutites, and siltstones) and the Neogene period (conglomerates, sandstones, arcilites, marlstones, with volcanic rocks, as tuff, interspersed lava, and diapirs) (Fig. 3). The surface geology is dominated by alluvial, fluvial-lacustrine, fluvioglacial, colluvial, lacustrine, moraine, and dune deposits from the Quaternary period (MMAyA, 2010). The study area has a slight inclination (mean slope: 3.8%) towards the northwest, which allows the flow of surface currents (IIS, 2013) (Fig. 3).

Lacustrine sediments overlap and are interspersed with fluvial sediments forming confining layers and consequently produce artesian conditions (Quaternary fluviolacustrine deposits) (IIS, 2013). Lacustrine sediments originated from the Pleistocene era until around 10,000B.P. (Before Present) (Servant-Vildary, 1993). The lacustrine plains (3800 m a.s.l.) have uniform deposition surfaces and do not reflect differentiated climatic events; their surface reflects traces of flood areas in rainy seasons (RASE), due to the remains of salt in different areas, left by temporary lagoons (MMAyA, 2010).

The mountainous surfaces (4100–4400 m a.s.l.) are represented among others by the volcanic hills with rounded shapes and medium slopes (MMAyA, 2010) (Fig. 3). The structural surfaces with relatively

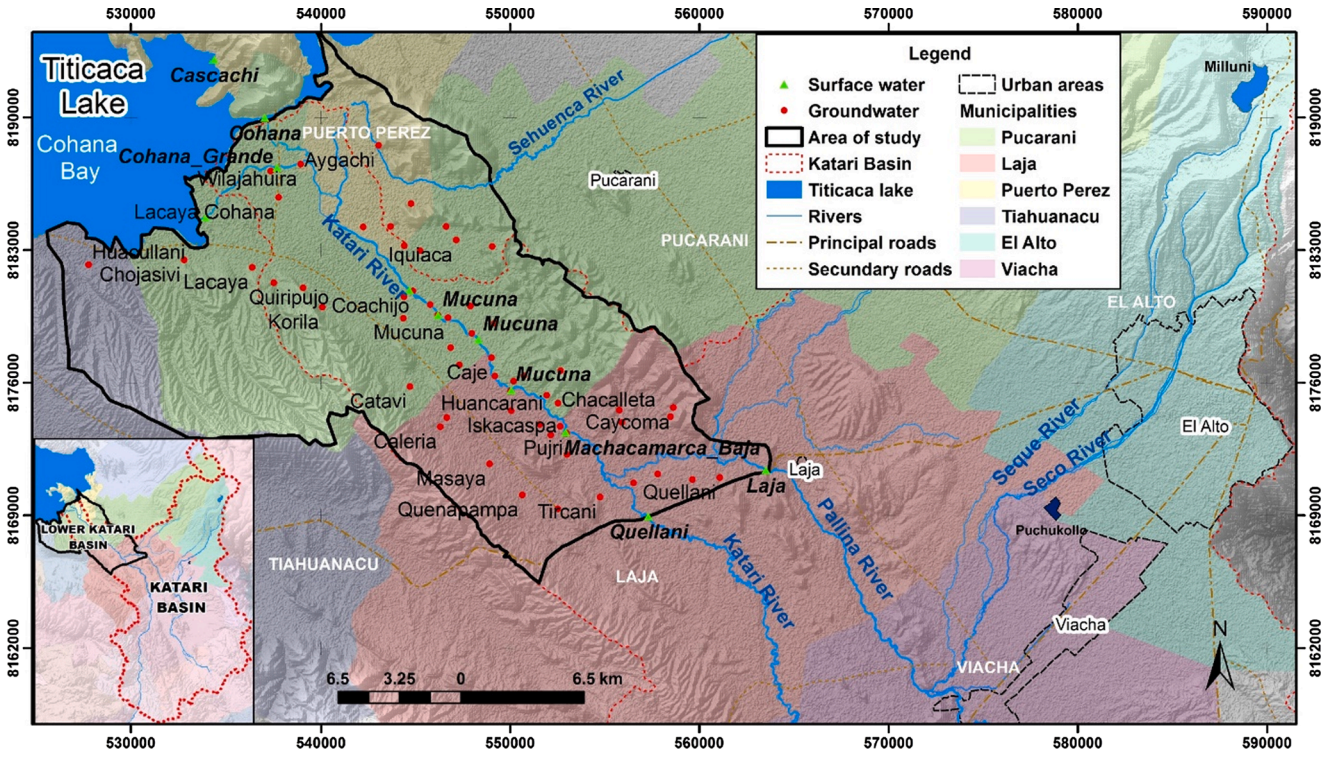

Fig. 2. Sampling points of the study area showing the important municipalities and urban areas.

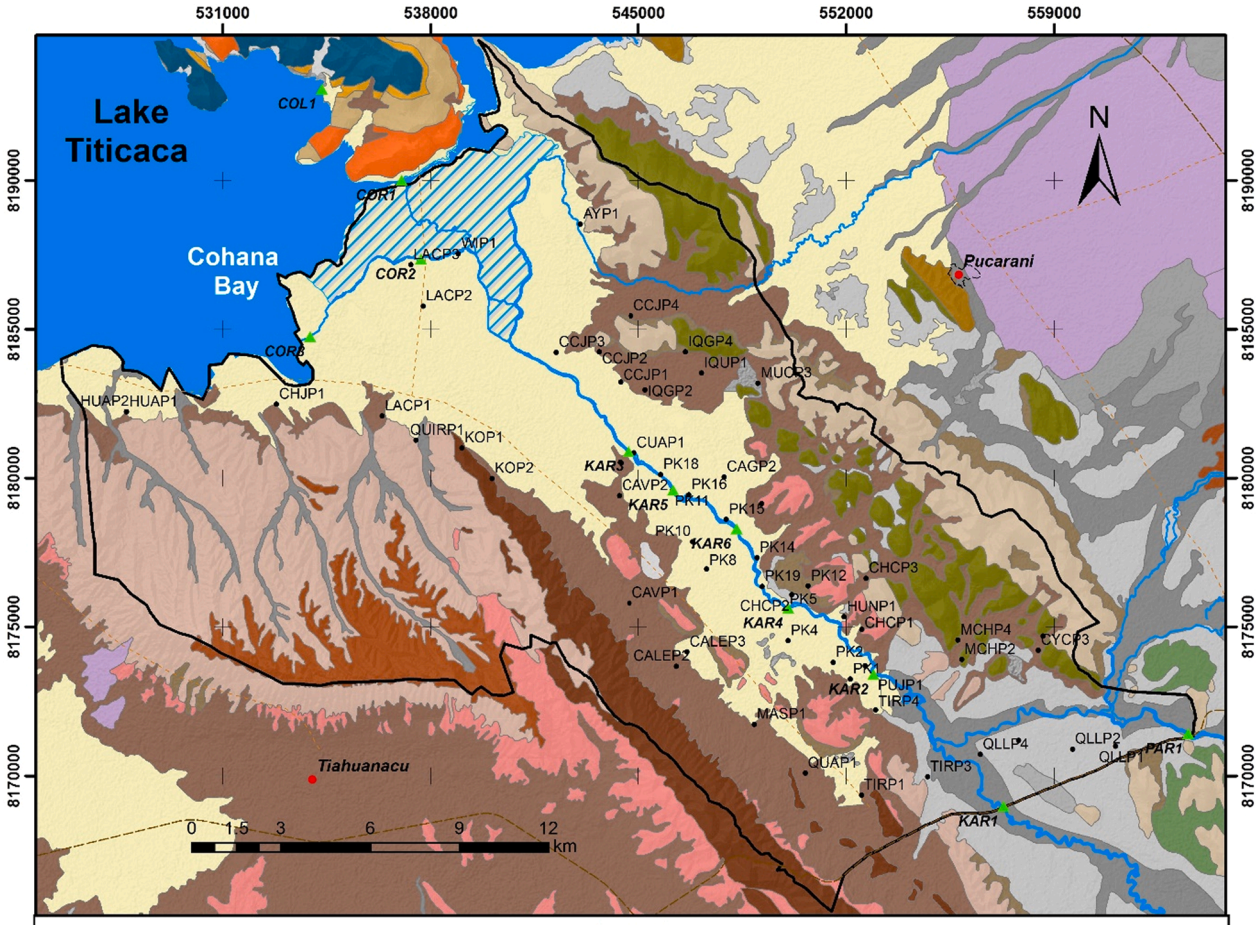

Legend

Surface water • Groundwater Area of study Delta Rivers Principal roads Secundary roads

Period	Formation	Description	Detail
Quaternary	Ql	Lacustrine Deposit	Slime, clay, sand.
Quaternary	Qfl	Lacustrine Fluvio Deposit	Gravels, sands, silts and clays.
Quaternary	Qcf	Coluvio-Fluvial Deposit	Gravels, sands, silts and clays.
Quaternary	Qfg	Fluvio-Glacial Deposit	Gravels, sands, clays.
Carboniferous	Ccum	Cumana Formation	Grayish green diamictites interspersed with sandstones, limolites and conglomerate levels.
Tertiary	Ttc	Taraco Formation	Conglomerates and red-orange sandstones.
Tertiary	Tcl	Cachilaya Formation	Polymythic conglomerates, reddish yellowish brown clays with tuff levels.
Tertiary	Tcnr	Terrace Deposit	Reddish polymythical conglomerates, and orange sandstone to violaceous.
Quaternary	Qt	Terraza deposnto	Boulders, gravels, sand, silt and clays.
Quaternary	Qa	Alluvial Deposits	Boulders, gravels, sand, silt and clays.
Quaternary	Qaa	Alluvial Spectrum Deposit	Boulders, gravels, sands and silt.
Permian	Pcc	Copacabana Formation	Gray to brown limestones, green marls to violaceas and brown sandstones.
Quaternary	Qg	Glacial Deposit	Blocks, gravels and clays.
Quaternary	Qc	Colluvial Deposit	Blocks and sand.
Carboniferous	Cks	Kasa Formation	Whitish to reddish sabulitic sandstone.
Tertiary	Tkk	Kollu Kollu Formation	Reddish-greenish sandstone, conglomerate lenses, clay plaster and tuffs.
Devonian	Dclp	Colpacucho Formation	Yellowish and reddish brown sandstones with gray limolite levels.
Devonian	Dbl	Belen Formation	Yellowish brown sandstone with brown limolite levels.
Devonian	Dw	Vila Vila Formation	Yellowish brown sandstone with brown limolite levels.
Quaternary	Qe	Eolian Deposit	Fine grained sand.
Quaternary	Qul	Ulloma Formation	Calcareous sands and clays.

Fig. 3. Geology and sampling point of the study area.

flat surface relief, which are composed of rocky outcrops, have an origin often related to the development of tabular geological formations, composed of volcanic-clastic spills, mostly of ignimbritic nature of whitish tones, slightly compact, associated with the volcanism of plio-pleistocene (MMAyA, 2010).

2.4. Hydrogeology

The mud schist is observed from the Devonian Silurian Paleozoic fences in the GW reservoir. The La Paz formation of Tertiary age is distributed above this reservoir, and the sediments of La Paz formation are formed in the aquifer (a formation with higher permeability that is formed of thick and unsorted materials). These sediments are from the Quaternary system represented by moraines and alluvial deposits (Fig. 3). There are GW resources under artesian conditions (confined) and phreatic conditions (IIS, 2013).

The sediments of the aquifer were mainly deposited by rivers that carry sediments from the Eastern Cordillera to the southwest (sediments finer than those in the eastern part), where better transmissibility conditions are found. This area is topographically variable with mountainous areas with high slopes (range from 45 to 66% on mean and in some cases $>$ 100%) and plains with relatively low slopes (mean slope: 3.8%), as well as with the presence of isolated hills. The water level is one meter below the surface, which forms swampy terrain as a result of flood during the RASE. The GW (by infiltration) from Katari Basin flows from the northeast side of mountainous areas. The estimated GW flow direction towards the southwest path and is discharged by evapotranspiration in topographically low areas (IIS, 2013).

3. Material and methods

3.1. Field investigations

Four sampling campaigns were carried out considering the first two during RASE (February 2016 and March 2017) and the other two in dry season (DRSE) (October 2016 and August 2017). The pH, temperature (T), electrical conductivity (EC), redox potential (E_h), total dissolved solids (TDS), dissolved oxygen (DO) (multiparameter portable meter HANNA-HI 9828) were measured in the field. The E_h values were corrected with respect to the hydrogen electrode (Appelo and Postma, 2005). The portable instruments were calibrated before the experiment, and all equipment was rinsed three times with deionized water. Alkalinity (quoted as HCO_3^-) was also determined on-site by titration with 0.16 N H_2SO_4 until the endpoint at pH 4, as indicated by a color change of a mixed acid-base indicator, using a microdosimeter (portable titrator) West Systems Hi Tech Devices RGD. Geographical coordinates were recorded at each site using a handheld GPS GARMIN GPS12^{TM}.

3.1.1. Piezometer installation

A network of monitoring wells (piezometers) was installed in the lower area of LKB on the Katari River, to estimate the hydrogeological characteristics of shallow GW systems of the Katari River, effluents, and tributaries. The lithological profile and systematic description of the ground character throughout the monitoring network were estimated by the emphasis on the flood plain (area of the high probability of interaction between SW and GW) and the consequent collection of sediment and GW samples. In details, seventeen (n = 17) monitoring wells (piezometers) were installed in the central flat area (10 km) along the Katari River, including the villages Pujri, Masaya, Caleria, Catavi, Chacalleta, Huancarminto, Caje and Mucuña. The Katari River overflows frequently in this region lower gradient of elevation (mean slope: 3.8%). In addition, eleven communal wells close to the piezometers were identified to be monitored. This network of monitoring wells was used for the development of a shallow hydrogeological study of the sector, which allows establishing (i) the quality of GW consumed in the area, (ii) the direction of water flow, and (iii) interaction between the SW and GW.

The piezometers were installed manually with rotation and pressure by augers of 3 in. and recorded the phreatic level as well as the lithological profile during sediment extraction. The representative samples (sediments per layer and water) of the saturated and unsaturated zone were collected for further analysis in the laboratory. The design scheme of the monitoring wells is adapted according to Nielsen (1991).

3.2. Water sampling

3.2.1. Groundwater samples

A total of 206 samples were collected, in RASE 46 samples were taken in February 2016 (FEB16GW) and 59 samples in March 2017 (MAR17GW). In DRSE for a seasonal comparison, 43 samples were collected in October 2016 (OCT16GW) and 58 samples in August 2017 (AUG17GW). Water samples from 17 installed piezometers were collected during the same field campaigns. Samples were taken with a bucket or pump, depending on the type of well. The bucket was rinsed with well water before the collection of water samples. The piezometers were purged continuously for at least ten minutes to stabilize field parameters. Depth of 'well' and water column were measured in the field with a water level meter (Solinst 101) (where possible) and both measurements were made on all piezometers. The depth, construction type, and characteristics of the 'well' changed over time (water level, sediment at the bottom of the well, organoleptic properties), and those were obtained from the owner of the 'well'.

Water samples were collected for laboratory analysis following the procedure described in Bhattacharya et al. (2002b). Samples were filtered using Sartorius 0.45 μm filters and the water samples were collected in three replicates from each site, three bottles of 80 mL for anions, cations/TEs, and As speciation. The samples (for the cations/TEs and As speciation analysis) were acidified using 1% v/v HNO_3. As speciation was performed with Disposable Cartridges (MetalSoft Center, USA), the samples were passed through the cartridge that retains all As (V) following the methodology described by Meng et al. (2001). All samples were stored in a refrigerator at 4 °C until laboratory analyses.

3.2.2. Surface water samples

Nine water samples were collected in each campaign along the Pallina and Katari rivers to CB during the RASE: February 2016 (FEB16SW) and March 2017 (MAR17SW). Eight samples were taken in October 2016 (OCT16SW) and eleven samples in August 2017 (AUG17SW) from the same sites during the DRSE for a seasonal comparison. Samples were taken from the middle of the river channel, with a plastic bucket rinsed three times with river water, following the same procedure as for GW. The river flow was measured at each sampling point, as well as other hydrological data such as cross-section (width, maximum depth, wet section, and wet perimeter) and mean surface speed.

3.3. Sediment sampling

3.3.1. Core sediment

A total of 54 sediment samples (e.g. PK16-1, PK16-2, PK16-3, and PK16-4) were collected from seventeen piezometers (PK1–PK19) to estimate the log profiles of piezometers. The sediment samples were characterized by color, grain size, and texture and were stored in zip-lock bags to transport for subsequent laboratory studies.

3.3.2. River sediment

A total of 17 sediment samples (8 in March 2017 and 9 in August 2017) were collected at the same sampling site as river water samples to compare water and sediment chemistry (Fig. 2). The samples were taken with a shovel from a riverbed in the middle of the streamflow at a depth of 0.3 m and were stored in plastic zip-lock bags.

3.4. Laboratory investigations

3.4.1. Chemical analysis of water

Major anions (Cl^-, SO_4^{2-}, NO_3^-, PO_4^{3-} and F^-) were measured by ion chromatography (Dionex - ICS 1100) at the Environmental Chemistry Laboratory at the Universidad Mayor de San Andrés (UMSA) in La Paz, Bolivia. Major cations (Ca^{2+}, Mg^{2+}, Na^+, and K^+) and TEs (Si, As, Al, B, Br, Cu, Fe, Li, Mn, Pb, Sr, Cr, Ba, and Zn) of the samples were determined by inductively coupled optical emission spectrometry (ICP-OES; Varian Instruments, model Varian Vista Pro Ax) at the laboratory of the Department of Geology Sciences, Stockholm University, Sweden. The As-speciation samples gave the As(III) concentration and subtraction from the As_{Tot} in the TEs samples then gave the amount of As(V). The quality assurance control of major ion analyses was ensured through the estimation of charge balance error (CBE). The most of samples were in an acceptable CBE of ±10%. Certified reference material (NIST SRM 1640a - Trace Elements in Natural Water) was used to check the accuracy. Replicate analyses were carried out to check the precision of the results, accuracy, and precision indicated variations within the range of ±10%.

3.4.2. Core sediment and river sediment analysis

The determination of physical and chemical parameters in CS and RS were carried out at the Hydrochemistry Laboratory - IIQ at the Universidad Mayor de San Andrés (UMSA) in La Paz, Bolivia. A total of 71 sediment samples (54 CS and 17 RS) were dried at room temperature for 3 weeks, turning the samples for rapid moisture removal. Moisture determination was carried out by a gravimetric method (McKean, 1993). One gram of sifted dry sample (0.5 mm) was weighed, and then the sample was dried again in an oven at 105 °C for 24 h. At the end of the process, the sample was cooled in a desiccator for 18 h and the samples were reweighed, and the humidity was calculated by gravimetric difference. The EC and pH were measured with the potentiometric method (Chilón, 1996), using a model WTW EC and pH meter.

The organic carbon (OC) content was determined by the wet combustion method of Walkey and Black, digesting the samples in sulfuric acid and potassium dichromate and then they were titrated with ferrous sulfate (Black, 1965). The standardized method of the Bouyoucos densimeter was used for the textural determination (Chilón, 1996), which consists of the variation in the sedimentation rate of the sample particles according to their size. Finally, sediment color according to the Munsell color system was determined on wet and dry samples.

3.4.3. Pseudo total extraction of sediments

A total of 71 sediments samples (CD and RS) were digested using a digester VELP DK-20 (open digestion system) to quantify the total content of trace elements by digesting 0.5 g of sample in a mixture of 3 mL of HNO_3 (65% m/v) and 3 mL of HCl (37% m/v), both purified by sub-boiling distillation. The sample was quantitatively transferred to a digestion tube (Kjeldahl digestion) with glass balls to prevent eruptive boiling and was boiled in the digester with a programmed digestion ramp (Table 1). The extract was cooled and diluted to a total volume of 50 mL with deionized water, then filtered through a filter paper (Whatman grade 44) and stored in plastics bottles. Sediment extracts were analyzed with an ICP-OES, at the Department of Geology Sciences, Stockholm University, Sweden.

3.4.4. Sequential extraction

Sequential extraction was performed on the 54 core sediment samples using the BCR method (Community Bureau of Reference, superseded by the Standards, Measurements and Testing Programme of the European Community) (Ure et al., 1993). This procedure was modified in concentrations, pH, and reagent volumes according to the procedure developed by Cáceres Choque et al. (2013).

Fraction 1 (F1- Exchangeable + acid soluble fraction). 0.5 g of sample in 20 mL of acetic acid (0.11 M) was added in a tube. The mixture was shaken for 16 h in a mechanical stirrer at room temperature (18 °C) and separated from the solid phase by centrifugation at 3000 rpm for 1 h. The supernatant was decanted in a plastic bottle and the residue was washed with 10 mL of deionized water, shaken for 15 min, and centrifuged again (3000 rpm) for 15 min. The supernatant was carefully removed and the solid phase was saved for the next extraction.

Table 1
Digestion are ramps used in the open digestion system (pseudo total extraction of sediments).

Ramp used (Digester VELP DK-20) T (°C)	Time (min)
25	5
40	5
80	30
100	120

Fraction 2 (F2 - reducible fraction). 20 mL of 0.5 M hydroxylamine hydrochloride (adjusted to pH 1.5 with nitric acid 10%) was added to the solid phase of fraction 1. It was shaken for 16 h at 3000 rpm at room temperature (18 °C) for 1 h. The extract was separated from the solid phase by centrifugation, as described in step 1.

Fraction 3 (F3 - oxidizable fraction). 5 mL of 8.8 M hydrogen peroxide (adjusted pH 2) was added to the fraction 2 residue in a centrifuge tube. It was covered and digested at room temperature for 1 h with occasional manual shaking. The tube was digested again 1 h to 85.5 °C in a water bath until the volume was reduced to 2 mL. Then 5 mL of hydrogen peroxide was added, covered, and heated again to 85.5 °C, the volume was reduced to 1 mL. After cooling, 50 mL of ammonium acetate (adjusted pH 2 with nitric acid) was added, and the tube was shaken for 16 h at room temperature. The extract was separated from the solid phase by centrifugation as described in steps 1 and 2.

Fraction 4 (F4 - residual fraction). The final residue at the end of the BCR procedure was digested with 20 mL of aqua regia for 16 h and boiled on a sand bed for 3 h to 95–100 °C. The extract was separated from the solid phase by centrifugation, as described in steps 1, 2, and 3.

The extracts obtained in each step were analyzed using an atomic absorption spectrometer Perkin Elmer AAnalyst 200 with flame atomization (air/acetylene) for high element content and electrothermal atomization in graphite furnace HGA 800 for lower concentrations at the Hydrochemistry Laboratory of the Universidad Mayor de San Andrés in La Paz, Bolivia. The precision and exactitude of analysis were tested by internal quality control of the laboratory. Reference material (MR-C17-2 of CAEAL stands for Canadian Association for Environmental Analytical Laboratories) was used to check the exactitude, and duplicate analyses were carried out to check the precision of the results, exactitude and precision indicated variations within the range of ± 15% with some exceptions.

3.5. Data analysis

3.5.1. Hydrochemical data analysis of water

The values of variables that were below the detection limit, (bdl) or "<DL", were changed to the values equal to the detection limit divided by two, with the following expression "DL/2″ for their treatment in all calculations, according to methodology suggested by Farnham et al. (2002). The Diagrammes software 6.59 (Laboratoire d'Hydrogéologie d'Avignon, 1999) was used to create the Piper plots, Aqueachem software 4.0.264 (Waterloo Hydrogeologic Inc, 2003) was used to create the Stiff and Box and Whisker plots and to determine water type. The aqueous speciation of As (saturation indices and distribution of species) in water samples was calculated using the PHREEQC software (Parkhurst and Appelo, 1999), using the MINTEQ database (minteq.dat) which includes a thermodynamic database for As.

3.5.2. Spatial analysis

The tools of the Geographic Information Systems (GIS) were applied to data, selected parameters were directly spatialized for SW and the Kriging method (advanced geostatistical procedure) (Esri, 2016) was used for GW. The Geometrical Interval Classification (GIC) method (class ranges based on intervals that have a geometric sequence based on a multiplier), was used to visualize continuous data and produces a visually appealing and cartographically complete result (Esri, 2008); these procedures were done in ArcGIS 10.2.2 software.

4. Results

4.1. Quantitative spatial–temporal variation of water

The main characteristics of GW and SW (wells, piezometers, rivers, and lake) in different sampling locations are presented in Table 2. The field measurements (statistical summary), concentrations of major ions, and TEs are shown in Table 3. The depth to the GW level in the study area varies considerably between RASE in FEB16GW (mean: 2.4 m; range: 0.3–6.7 m) and in MAR17GW (mean: 2.9 m; range: 0.4–9.2 m), DRSE in OCT16GW (mean: 2.9 m; range: 0.4–8.2 m) and in AUG17GW (mean: 2.9 m; range: 0.2–9 m) as can be observed in the Fig. 4a, b, c, d, respectively. The increase of the GW level from 0.2 to 0.5 m in RASE is observed in the wells and piezometers of the study area (Fig. 4a). However, the PK2 piezometer located in Iskacaspa (flat area) showed GW levels that vary by one meter between sampling campaigns (August 2015, February 2016, July 2016, March 2017, and August 2017) (Fig. 4b).

The spatial variation of the GW level in the study area varies from the area of the terraces (greater depth) to the flat area (lesser depth) (Fig. 4c, d), except in the area near Lake Titicaca. The seasonal variation between FEB17GW (RASE) (Fig. 4c) and AUG17GW (DRSE) (Fig. 4d) is also evident. It is also observed that the direction of preliminary flow follows the course from the hills (recharge area) to terraces and from terraces to the flat area (Katari River), and finally, the trend indicates that the direction of the flow is directed to Lake Titicaca (Fig. 4c, d) according to GW level in piezometers and wells. There is a great variation in the flow of water in rivers (Fig. 4c, d, e) considering the temporal variation (mean: 4 m^3/s; range: 0.9–5.1 m^3/s), especially after the confluence between Pallina and Katari rivers.

The water flow of the Katari River varies only 1 m between the seasons (RASE and DRSE) before the confluence with the Pallina River and this shows the great impact of the water flow of the Pallina River in the study area. The possible interaction of SW with GW could be occurring 25 km (KAR3) away downstream of the study area (Fig. 4e), due to the decrease in the flow values in both periods (RASE and DRSE); precisely, this is the region (flat), where floods occur due to the low slope of terrain (mean slope of plain 3.8%), also the GW level in the area is shallow (Fig. 4c, d). The interaction of SW with GW is verified considering the flow direction of GW, and it follows the same course of SW. There are some sectors such as Chacalleta and Huancarani, where could be direct interaction of SW with GW. This hypothesis is supported by the shallow depth of GW levels in the wells of this area, and the proximity of the wells to the course of the Katari River (e.g. CUAP1 10 m). Another probable explanation for the decrease in flow rates in this sector could be the greater evaporation of SW and consequently the reduction of water flow that increases the evaporation ratio, generating a reduction in its quantity, especially in DRSE.

The drag of solid material by Pallina River significantly affects the Katari River along its course after their confluence. This process is increased in the central and northwest region of the basin, in the regions of low slope, where solid materials (garbage) are deposited along the banks in DRSE and then are washed away in RASE. In RASE, the Katari River is often overflowed by extreme events that originate from the increase in precipitation upstream of the basin, causing large floods downstream of the basin, disseminating all the solid material that drags

Table 2
Location and main characteristics of sampling sites (water and sediment) in the study area.

Groundwater (GW)											
Code	Location	Type	Well Depth (m)	Code	Location	Type	Well Depth (m)	Code	Location	Type	Well Depth (m)
AYP1	Aygachi	Excavated	2.8	IQGP4	Iquiaca	Excavated	3.7	PUJP1	Pujri	Excavated	3.9
CAGP1	Caje	Excavated	3.3	IQUP1	Iquiaca	Excavated	6.7	QLLP1	Quellani	Excavated	6.0
CAGP2	Caje	Excavated	3.2	ISKP2	Iskacaspa	Excavated	2.9	QLLP2	Quellani	Excavated	8.8
CALCHP1	Calachaca	Excavated	1.8	KOP1	Korila	Excavated	1.6	QLLP3	Quellani	Excavated	12.8
CALEP1	Caleria	Excavated	4.0	KOP2	Korila	Excavated	0.8	QLLP4	Quellani	Excavated	3.3
CALEP2	Caleria	Excavated	6.6	LACP1	Lacaya	Excavated	1.7	QUAP1	Quenapampa	Excavated	6.5
CALEP3	Caleria	Drilled	ND	LACP2	Lacaya Cohana	Excavated	ND	QUIRP1	Quiripujo	Excavated	2.3
CAVP1	Catavi	Excavated	9.7	LACP3	Lacaya Cohana	Excavated	ND	TIRP1	Tircani	Excavated	2.2
CAVP2	Catavi	Excavated	4.2	MASP1	Masaya	Excavated	2.8	TIRP2	Tircani	Excavated	3.7
CAVP3	Catavi	Excavated	2.6	MCHP1	Machacamarca	Excavated	3.2	TIRP3	Tircani	Excavated	3.1
CCJP1	Coachijo	Excavated	1.9	MCHP2	Machacamarca	Drilled	ND	TIRP4	Tircani	Excavated	5.9
CCJP2	Coachijo	Excavated	3.3	MCHP4	Machacamarca	Excavated	3.5	WIP1	Wilajahuira	Excavated	ND
CCJP3	Coachijo	Excavated	2.5	MUCP3	Mucuña	Excavated	4.7	Surface water (SW)			
CCJP4	Coachijo	Excavated	4.7	PK1	Iskacaspa	Drilled	2.9				
CHCP1	Chacalleta	Excavated	3.3	PK10	Caleria	Drilled	2.7	Code	Location	Description	Code (sediment)
CHCP2	Chacalleta	Excavated	2.5	PK11	Catavi	Drilled	3.7				
CHCP3	Chacalleta	Excavated	3.6	PK12	Chacalleta	Drilled	5.4	COL1	Cascachi	Titicaca Lake	
CHJP1	Chojasivi	Excavated	1.7	PK14	Caje	Drilled	3.3	COR1	Cohana	Katari River	KAS7
CUAP1	Coachijo	Excavated	2.4	PK15	Caje	Drilled	2.8	COR2	Lacaya	Katari River	COS2
CYCP1	Caycoma	Excavated	3.2	PK16	Mucuña	Drilled	4.0	COR3	Calachaca	Katari River	COS3
CYCP2	Caycoma	Excavated	5.0	PK18	Coachijo	Drilled	3.2	KAR1	Quellani	Katari River	KAS1
CYCP3	Caycoma	Excavated	6.1	PK19	Chacalleta	Drilled	3.4	KAR2	Pujri	Katari River	KAS2
HUAP1	Huacullani	Drilled	ND	PK2	Iskacaspa	Drilled	3.3	KAR3	Catavi	Katari River	KAS3
HUAP2	Huacullani	Drilled	ND	PK4	Masaya	Drilled	2.8	KAR4	Chacalleta	Katari River	KAS4
HUNP1	Huancarani	Excavated	2.9	PK5	Masaya	Drilled	3.1	KAR5	Catavi	Katari River	KAS5
IQGP1	Iquiaca	Excavated	4.0	PK6	Masaya	Drilled	4.2	KAR6	Caleria	Katari River	KAS6
IQGP2	Iquiaca	Excavated	4.2	PK8	Caleria	Drilled	2.6	PAR1	Laja	Pallina River	PAS1

ND: not determined, PK: piezometer.

Table 3
Statistical summary of field-measured parameters in groundwater and surface water.

	Rainy season (RASE)								Dry season (DRSE)							
	February 2016 (FEB16GW)				March 2017 (MAR17GW)				October 2016 (OCT16GW)				August 2017 (AUG17GW)			
	Groundwater (GW) (n = 46)				Groundwater (GW) (n = 59)				Groundwater (GW) (n = 43)				Groundwater (GW) (n = 58)			
Parameter	Min	Max	Mean	SD	Min	Max	Mean	SD	Min	Max	Mean	SD	Min	Max	Mean	SD
pH	6.6	9.2	7.9	0.6	6.4	8.3	7.2	0.4	6.6	9.6	7.4	0.6	7.2	8.8	7.9	0.4
EC (μS/cm)	145.0	22470.0	2453.6	3993.1	125.0	13220.0	1799.3	2631.6	111.0	23850.0	2813.6	4612.4	125.0	11740.0	1773.4	2353.3
Eh (mV)	155.0	259.9	209.3	29.7	221.7	537.0	278.5	53.8	234.7	274.7	251.5	10.2	235.4	274.0	247.2	6.5
T (°C)	12.7	19.0	14.6	1.3	11.0	17.3	14.1	1.3	11.2	18.8	14.4	1.9	4.4	15.6	11.5	2.1
TDS (mg/L)	72.0	11220.0	1227.6	1994.9	63.0	6600.0	911.4	1327.0	56.0	11930.0	1422.8	2332.0	63.0	4363.0	797.1	969.2
DO (mg/L)	0.2	75.7	4.7	10.9	0.6	89.4	5.2	11.4	0.3	11.4	4.2	2.7	1.2	13.1	4.0	2.1
HCO_3^- (mg/L)	28.2	670.1	243.1	121.5	58.6	661.3	235.9	111.3	68.1	644.2	263.6	107.3	65.9	527.0	264.3	103.0
Cl^- (mg/L)	2.6	3030.1	362.5	656.2	0.6	3083.8	276.9	583.6	2.4	2313.3	353.4	619.6	3.8	2568.0	268.9	507.1
SO_4^{2-} (mg/L)	11.7	2034.0	300.3	453.5	7.5	2056.2	199.0	364.4	6.7	2515.9	371.2	580.2	7.4	2149.9	267.1	456.4
NO_3^- (mg/L)	0.5	340.6	26.5	56.5	0.2	243.6	12.9	34.1	0.2	283.6	16.4	45.1	0.1	228.2	18.4	37.7
PO_4^{3-} (mg/L)	0.004	1.0	0.3	0.3	0.01	2.2	0.1	0.4	0.01	11.1	0.4	1.7	0.01	4.1	0.2	0.6
F^- (mg/L)	ND	ND	ND	ND	0.09	1.9	0.4	0.4	0.02	0.7	0.1	0.1	0.01	1.1	0.2	0.2
Ca^{2+} (mg/L)	9.6	411.7	102.8	92.5	12.7	464.4	82.4	78.6	12.4	465.5	117.0	102.4	13.6	462.0	105.7	94.2
Mg^{2+} (mg/L)	6.1	207.6	34.9	36.5	5.5	211.9	34.1	39.1	3.1	200.3	37.4	45.7	2.4	153.7	30.8	32.7
Na^+ (mg/L)	4.6	1820.1	239.5	377.8	4.2	1825.5	169.7	320.2	4.3	1718.9	263.1	400.4	4.5	1662.7	176.1	314.6
K^+ (mg/L)	2.5	50.9	14.3	13.9	2.3	49.7	12.4	11.1	1.6	51.5	13.9	12.9	2.7	42.7	13.2	9.9
Si (mg/L)	3.4	21.1	13.3	4.6	0.2	19.4	10.3	4.4	1.9	21.5	11.0	4.3	1.0	18.1	10.2	4.0
Al (μg/L)	0.5	254.1	26.0	58.8	1.9	440.8	25.6	64.7	1.1	269.7	30.1	59.1	5.3	4394.5	104.3	575.7
As (μg/L)	0.8	60.7	11.6	11.7	0.8	253.5	24.5	43.2	0.8	110.5	18.2	26.3	0.8	288.5	24.8	51.0
B (μg/L)	93.0	716.2	383.7	119.1	93.3	2016.6	400.5	342.9	100.4	1292.1	321.9	215.5	96.5	2472.9	452.6	442.0
Ba (μg/L)	2.3	346.4	47.8	53.8	5.4	291.7	74.4	58.0	8.3	297.5	76.2	54.6	6.5	298.6	81.0	59.2
Cu (μg/L)	0.3	12.5	2.2	2.4	0.8	20.5	3.5	3.1	0.3	13.0	4.5	3.2	1.2	15.5	4.4	2.9
Fe (μg/L)	0.2	56.5	6.8	11.0	3.2	1322.0	82.6	236.5	0.9	1104.4	66.4	179.1	7.8	2444.8	150.8	418.1
Li (μg/L)	3.9	669.6	63.6	103.3	1.9	583.5	49.4	79.7	2.0	687.8	56.7	103.4	1.8	176.1	41.3	37.5
Mn (μg/L)	0.04	967.0	98.4	220.7	0.6	6607.1	601.5	1443.1	0.1	4250.7	445.5	967.4	0.6	7259.3	596.9	1363.1
Mo (μg/L)	0.3	20.4	4.2	4.7	0.3	20.8	3.9	4.3	0.3	23.1	4.5	5.1	0.3	77.6	4.4	10.1
Sr (μg/L)	31.7	3663.0	703.7	758.3	81.6	4600.8	926.9	936.4	75.9	4845.3	920.6	895.9	88.1	4746.3	1055.4	1031.1
Ti (μg/L)	0.2	4.0	2.1	0.8	0.2	3.0	1.6	0.6	0.2	7.0	2.0	1.2	0.2	5.6	1.7	1.0
Zn (μg/L)	0.5	1427.2	100.0	290.4	1.8	293.7	13.8	38.8	0.8	113.0	11.1	19.0	4.2	78.4	12.8	14.4
	February 2016 (FEB16SW)				March 2017 (MAR17SW)				October 2016 (OCT16SW)				August 2017 (AUG17SW)			
	Surface water (SW) (n = 9)				Surface water (SW) (n = 9)				Surface water (SW) (n = 8)				Surface water (SW) (n = 11)			
pH	6.7	8.1	7.4	0.4	7.1	8.0	7.4	0.3	8.3	9.8	8.7	0.5	8.6	10.1	9.5	0.5
EC (μS/cm)	328.0	1443.0	638.9	343.0	389.0	2520.0	758.8	680.3	1444.0	2023.0	1703.2	161.3	970.0	2454.0	1320.1	406.9
Eh (mV)	210.0	266.3	251.5	17.2	264.1	275.1	269.4	3.3	244.8	270.7	251.8	8.5	243.8	249.2	246.7	1.6
T (°C)	16.8	21.6	19.0	1.7	11.6	18.2	14.1	2.0	16.0	22.4	19.4	2.2	7.7	16.8	12.9	3.4
TDS (mg/L)	164.0	721.0	346.3	172.8	193.0	1276.0	380.8	345.4	722.0	1010.0	851.1	80.1	484.0	1229.0	660.0	204.1
DO (mg/L)	1.6	7.4	4.4	1.6	0.7	7.1	4.3	2.0	8.7	18.6	14.1	4.2	5.8	22.0	12.3	5.3
HCO_3^- (mg/L)	60.3	219.6	132.6	44.0	87.8	246.4	142.3	56.8	136.6	544.2	381.4	136.0	164.7	461.2	315.4	78.7
Cl^- (mg/L)	19.6	420.6	105.9	121.7	21.3	426.5	87.1	129.4	75.9	181.1	138.0	44.8	55.9	224.4	140.9	54.2
SO_4^{2-} (mg/L)	21.5	244.0	101.9	64.6	31.9	333.4	92.3	95.8	68.9	462.8	132.8	134.3	45.3	506.0	197.9	138.8
NO_3^- (mg/L)	1.8	7.0	3.5	1.8	0.02	4.2	2.2	1.3	0.5	7.8	2.2	2.4	0.5	3.6	1.9	1.1
PO_4^{3-} (mg/L)	0.01	4.1	1.4	1.3	0.01	3.0	0.5	1.1	0.01	17.4	11.0	6.2	0.01	11.8	4.2	3.5
F^- (mg/L)	ND	ND	ND	ND	0.09	0.5	0.2	0.1	0.04	0.09	0.07	0.02	0.09	0.7	0.2	0.2
Ca^{2+} (mg/L)	28.4	82.2	49.7	20.6	21.8	101.8	45.4	26.5	26.0	89.2	55.1	17.8	57.3	116.9	65.9	17.1
Mg^{2+} (mg/L)	2.1	80.6	18.6	24.0	6.6	86.8	19.3	25.7	5.3	60.1	21.7	16.8	14.8	46.1	21.4	9.3
Na^+ (mg/L)	15.1	214.7	70.3	60.9	25.4	271.6	64.4	79.4	79.9	230.2	140.5	47.9	77.9	216.7	150.0	50.1
K^+ (mg/L)	1.6	25.2	9.9	8.1	5.0	29.5	9.3	7.7	3.2	34.6	21.0	12.4	7.7	27.1	19.2	6.4
Si (mg/L)	11.6	22.6	17.2	3.8	0.3	10.1	4.3	2.6	5.1	23.0	8.4	6.0	1.0	10.7	6.1	2.3

(*continued on next page*)

Table 3 (*continued*)

	Rainy season (RASE)								Dry season (DRSE)							
	February 2016 (FEB16GW)				March 2017 (MAR17GW)				October 2016 (OCT16GW)				August 2017 (AUG17GW)			
	Groundwater (GW) (n = 46)				Groundwater (GW) (n = 59)				Groundwater (GW) (n = 43)				Groundwater (GW) (n = 58)			
Parameter	Min	Max	Mean	SD	Min	Max	Mean	SD	Min	Max	Mean	SD	Min	Max	Mean	SD
Al (μg/L)	0.5	9.8	3.4	2.9	6.5	133.1	53.2	41.0	2.1	303.9	49.7	103.3	13.7	35.4	28.5	7.2
As (μg/L)	2.4	13.2	9.1	4.2	4.9	11.7	7.7	2.5	4.6	34.3	16.1	9.2	10.7	47.6	22.4	9.6
B (μg/L)	172.2	525.2	345.0	103.9	70.6	1711.1	313.6	539.3	111.4	361.0	222.0	104.5	142.5	966.1	237.1	242.8
Ba (μg/L)	9.2	181.4	68.4	59.2	38.7	86.0	55.8	16.4	13.4	82.1	37.0	21.9	14.3	55.0	29.9	11.3
Cu (μg/L)	0.7	7.4	2.2	2.1	1.4	4.2	2.6	0.8	1.0	14.9	4.5	4.3	2.7	4.3	3.3	0.5
Cr (μg/L)	0.2	2.2	1.0	0.7	ND	ND	ND	ND	0.2	1.3	0.7	0.4	0.2	1.0	0.5	0.3
Fe (μg/L)	1.0	14.7	3.7	4.3	5.5	150.9	56.8	45.5	2.6	305.5	58.7	101.2	19.8	70.9	38.3	13.5
Li (μg/L)	19.3	79.0	44.5	20.5	10.1	585.1	83.3	189.0	10.2	185.2	51.1	57.6	30.6	516.2	80.3	144.6
Mn (μg/L)	0.04	780.5	96.1	257.7	1.7	201.2	94.1	72.8	13.2	524.0	152.9	165.2	40.9	584.3	272.3	174.4
Mo (μg/L)	1.0	21.4	5.9	6.4	0.7	2.7	1.5	0.7	1.1	8.9	3.1	2.7	0.9	7.6	2.7	1.7
Sr (μg/L)	354.6	1541.4	831.6	397.4	154.7	1473.3	495.9	493.0	180.4	3022.5	723.0	972.1	455.8	1455.2	687.7	344.2
Ti (μg/L)	1.4	2.7	2.3	0.5	1.1	4.8	2.4	1.1	0.2	7.5	2.7	2.1	1.7	2.7	2.2	0.3
Zn (μg/L)	0.8	10.1	2.8		2.6	23.7	7.2	6.4	1.2	25.4	8.5	7.7	4.8	21.7	8.5	4.6

ND: not determined, SD: standard deviation.

the river. These events, although not frequent, generate a great environmental impact on the entire region, and populations near the course from the Katari River suffer due to the direct consequences.

4.2. Quantity and quality of drinking water

In general, 60% of the wells from LKB are used as drinking water and 30% of the wells are used alternatively when the drinking water distribution system does not work, whereas the remaining 10% of the wells are used for irrigation or animal consumption purpose. The northwest (Cohana - Wilajahuira), north (Aygachi - Iquiaca), east (Mucuña) and central sectors (flat area on the right side of the Katari River course) (Fig. 2) shows a scarcity of drinking water during DRSE.

The GW shows elevated salinity (EC), 35% (n = 46) of the all wells exceed the NB-512 (Bolivian regulation for drinking water) (1500 μS/cm) in FEB16GW (RASE), 30% (n = 43) in OCT16GW (DRSE), 31% (n = 59) in MAR17GW (RASE) and 28% (n = 58) in AUG17GW (DRSE). Arsenic concentration in GW are elevated, 39% and 44% of wells samples compare to NB-512 (10 μg/L) and WHO (10 μg/L) in FEB16GW and MAR17GW respectively, where both representing the RASE, finally 37% of wells sampled in OCT16GW and 40% in AUG17GW, both in the DRSE. The boron (B) values exceed the NB-512 (300 μg/L) in 84% of the wells in FEB16GW, 49% in MAR17GW, 42% in OCT16GW, and 48% in AUG17GW. 24% of all wells exceed the NB-512 (100 μg/L) of manganese (Mn) in FEB16GW, 40% in OCT16GW, 31% in MAR17GW, and 29% in AUG17GW.

The SW of the Pallina and Katari rivers are not suitable for human consumption due to elevated concentrations of As, B, Mn, Cl^-, SO_4^{2-} and EC compare to the NB-512, since the Pallina River transports industrial and wastewater from El Alto and Viacha cities. The natural water of Katari River are affected after receiving the water flow of Pallina River; observing the increase in the water flow (from 0.9 to 5.1 m^3/s) as seen in Fig. 4e, and also in water quality. In some cases, there are dilution processes of some elements (EC, SO_4^{2-}, Cl^-, Na^+) especially, in RASE.

4.3. Spatial-temporal variation of ground and surface water chemistry

4.3.1. pH, E_h, and EC

In GW, the pH is slightly alkaline and did not show great changes in both seasons (Table 3). E_h indicates oxidizing conditions Table 3. It was also observed that there is greater variability in the E_h ranges in RASE, whereas it was noticed more constant in the DRSE. E_h – pH diagram of the GW samples indicate that the $H_2AsO_4^-$ and $HAsO_4^{2-}$ are the dominant As species (Fig. 8a, b, c, d). In Fig. 8c and d, the stability in the E_h values is observed, even though the pH values slightly increased towards the alkalinity, which could be indicating a certain oxidizing system stability in the DRSE in comparison to the RASE.

There is a slight increase (1–10% in 2017) in EC in GW at RASE, especially in the south and flat area near the Katari River (Fig. 5a, b), which could indicate a greater dissolution of paleo-salts deposition. The EC in the terrace area is more stable (northeast and southwest from LKB) in both seasons. The salt deposits of the paleo-lakes and evaporative enrichment are responsible for high EC values in regions with sediments lacustrine origin and by evaporative concentration in a semi-arid climate (Servant-Vildary et al., 1993; Ormachea Muñoz et al., 2013; Ramos Ramos et al., 2012, 2014; Quino et al., 2019), these characteristics are especially present in the flat area of the basin (Fig. 5a, b).

In SW, The pH was noticed more alkaline in DRSE (Table 3). The E_h indicated an oxidizing condition (Table 3). The EC increases by 54% of the values in DRSE. The elevated values of EC were noted to be in the Katari River (upstream) and the Cascachi region (Lake Titicaca) (Fig. 5a, b) in both seasons. After the confluence of the Pallina River, there is a dilution effect in the values of EC.

4.3.2. Major ions

Data of major ions for GW samples were plotted in Box & Whisker

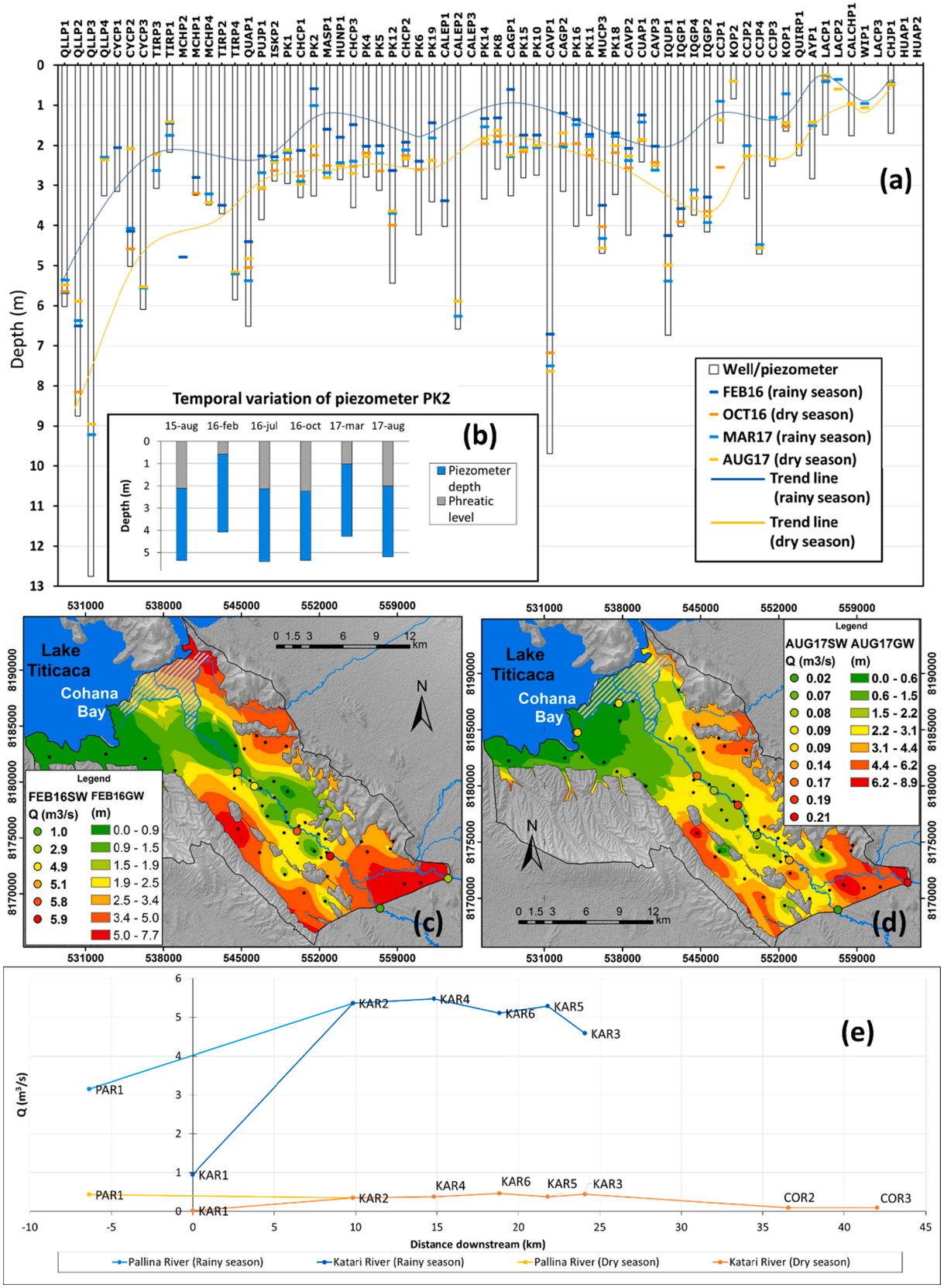

Fig. 4. Temporal variation of water column of the wells and piezometers in the study area: (a) and temporal variation (from August 2015 to August 2017) of PK2 piezometer; (b) Spatial and temporal variability of water column in groundwater (GW) and flow surface water (SW) in the rainy season (FEB16); (c) and dry season (AUG17); (d) Temporal variation of surface water in the study area (mean values) (e).

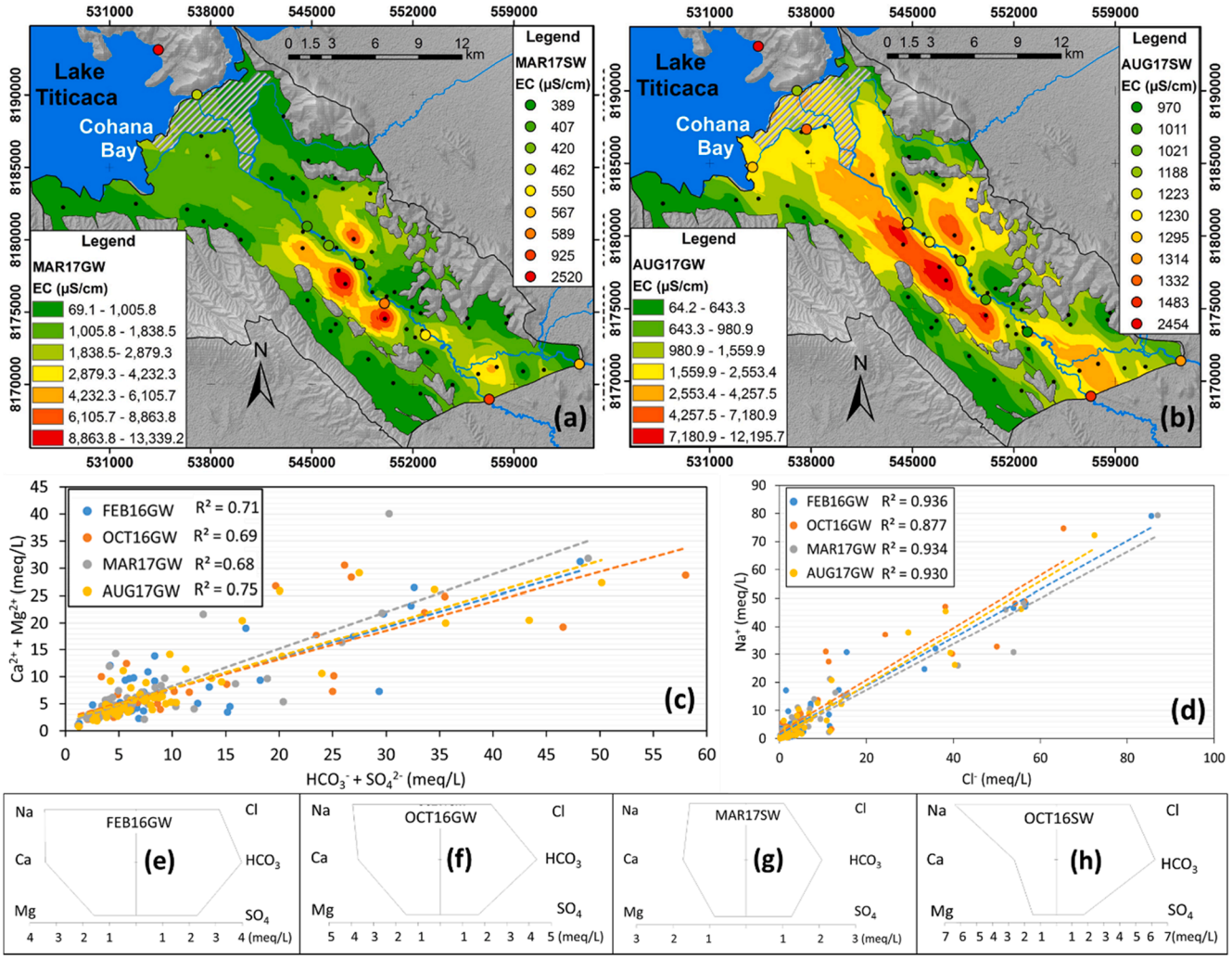

Fig. 5. Spatial and temporal variability of Electrical Conductivity (EC) in groundwater (GW) and flow surface water (SW) in the rainy season (MAR17); (a) and dry season (AUG17); (b) Bivariate plots for drinking water samples: $Ca^{2+}+Mg^{2+}$ *vs* $HCO_3^-+SO_4^{2-}$ (c) and Na^+ *vs* Cl^-; (d) in groundwater (GW), rainy season (FEB16 -MAR17) and dry season (OCT16 - AUG17). Stiff diagram of median groundwater (GW) and surface water (SW) in rainy season February 2016 GW (e) – March 2017 SW (g) and dry season October 2016 GW (f) – October 2016 SW (h).

(Fig. 6a, b), Stiff (Fig. 5e, f, g, h) and Piper diagrams; (Fig. 7a, b), where the major water type was identified in the shallow GW as Ca-HCO_3 (mean: 42% RASE and 50% DRSE), other as Na-Cl (mean: 24% RASE and 18% DRSE) and Na-HCO_3 (mean: 12% RASE and 14% DRSE). The composition of the remaining samples is more scattered as can be seen in the Piper diagram for FEB16GW (RASE) (Fig. 7a) and AUG17GW (DRSE) (Fig. 7b). There are two trends in geochemical evolution; one is towards Na-HCO_3 and the other towards Na-Cl in both seasons (Fig. 7a, b).

The Fig. 6a, b show the values of campaigns of RASE (FEB16GW) and DRSE (AUG17GW). The Na^+ and Cl^- ions were presented with the highest concentrations in RASE and in DRSE (Table 3) (Fig. 6a, b). Thus, the Na^+ and Cl^- are positively correlated in all campaigns (Fig. 5d), suggesting the dissolution of evaporated minerals such as halite, which is common in semi-arid areas (Quintanilla et al., 1995; Banks et al., 2004; Ramos Ramos et al., 2012, 2014; Ormachea Muñoz et al., 2016), confirmed by geochemical modeling (Fig. 8i).

The predominant ions such as HCO_3^- was noticed in RASE and in DRSE (Table 3) (Fig. 5e) along with other predominant ions such as Ca^{2+} was exhibited in RASE and in DRSE (Table 3) (Fig. 5e). The 'SO_4^{2-}+HCO_3^-' and 'Ca^{2+}+Mg^{2+}' showed a positive correlation (slope ~ 1) (Fig. 5c) and suggesting a possible source by weathering and/or dissolution of limestone (calcite), dolomite, and gypsum (Ramos Ramos et al., 2012, 2014; Ormachea Muñoz et al., 2013, 2016), this is confirmed by geochemical modeling (Fig. 8i).

The SO_4^{2-} concentration is an important anion in RASE and in DRSE (Table 3) due to the high salinity in GW. The elevated concentrations of NO_3^- indicated the existence of anthropogenic sources, especially in specified regions around the Pallina River, the confluence between the Katari and Pallina rivers, and near Lake Titicaca. The cations such as Mg^{2+} and K^+ have low concentration, compared to Ca^{2+} and especially to Na^+.

In Fig. 7a, b, the main water type was observed as Ca-HCO_3, as a predominant hydrochemical facies (Fig. 5e, f, g, h). However, the ions with the highest concentrations are Na^+ and Cl^- (Fig. 6a, b), as can be seen in the plotted values of total dissolved solids (TDS) corresponding to each point in the Piper diagrams (Fig. 7a, b).

The major ions for SW samples show in Box & Whisker, Stiff, and Piper diagrams (Fig. 6e, f; Fig. 5g, h; Fig. 7c, d). The major water type identified in the SW is Ca-HCO_3 (mean in RASE: 39%; mean in DRSE: 69%). There is a trend in geochemical evolution towards Na-HCO_3 in both seasons (Fig. 7c, d). Fig. 6e and f show the representative campaigns of FEB16SW and AUG17SW respectively, in RASE. All major ions occur in a range between 0.01 and 426.5 mg/L in RASE and between 0.01 and 544.2 mg/L in DRSE (Table 3). The increase of the concentrations in DRSE compared to RASE was 61% for HCO_3^-, 31% for Cl^-, 41% for SO_4^{2-}, 21% for Ca^{2+}, 12% for Mg^{2+}, 53% for K^+ and 54% for

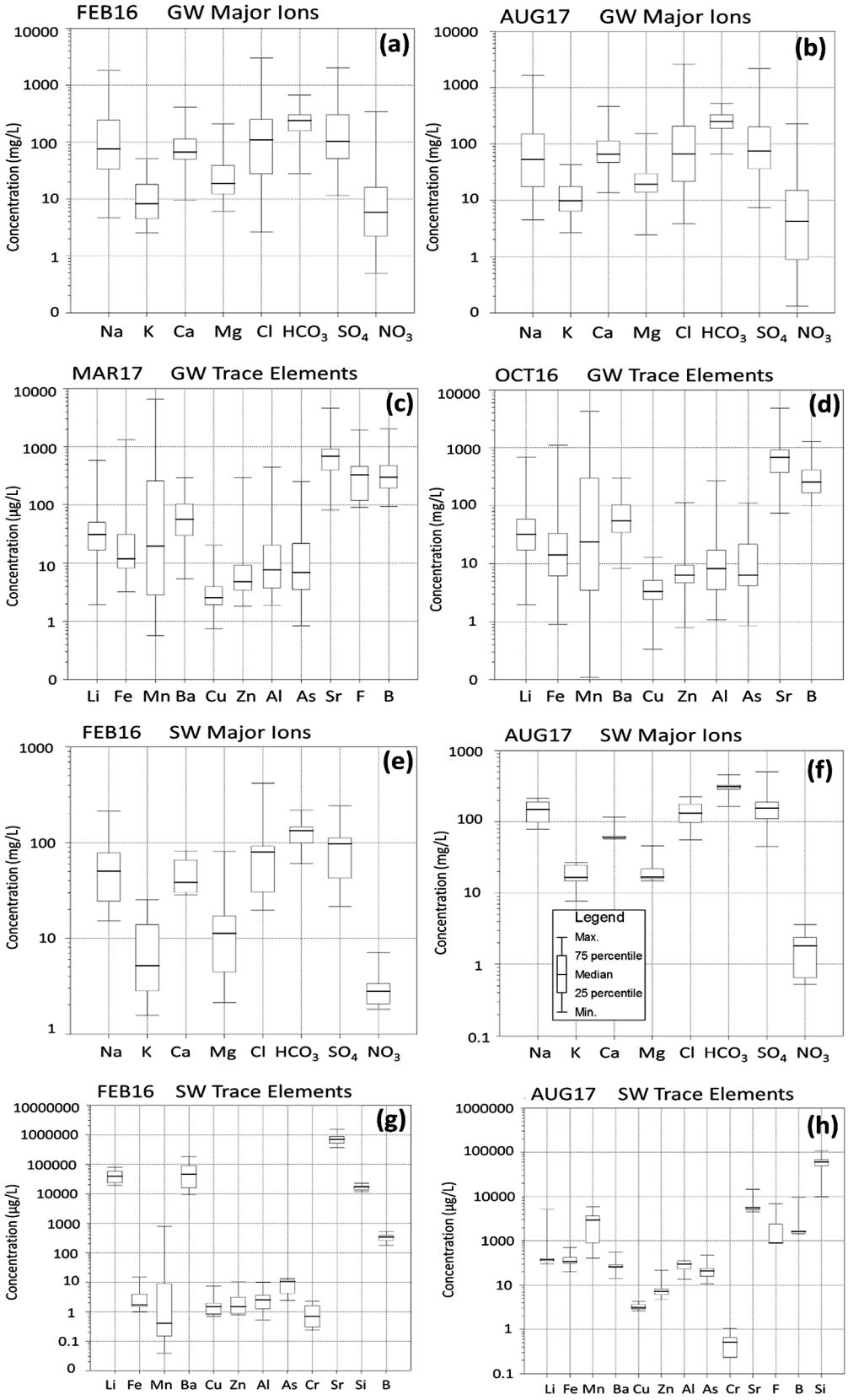

Fig. 6. Box & Whisker plot for the distribution of major ions in groundwater (GW): rainy season (FEB16) (a), and dry season (AUG17) (b). Trace elements in groundwater (GW): rainy season (MAR17) (c), and dry season (OCT16) (d). Major ions in surface water (SW): rainy season (FEB16) (e), and dry season (AUG17) (f). Trace elements in surface water (SW): rainy season (FEB16) (g), and dry season (AUG17) (h).

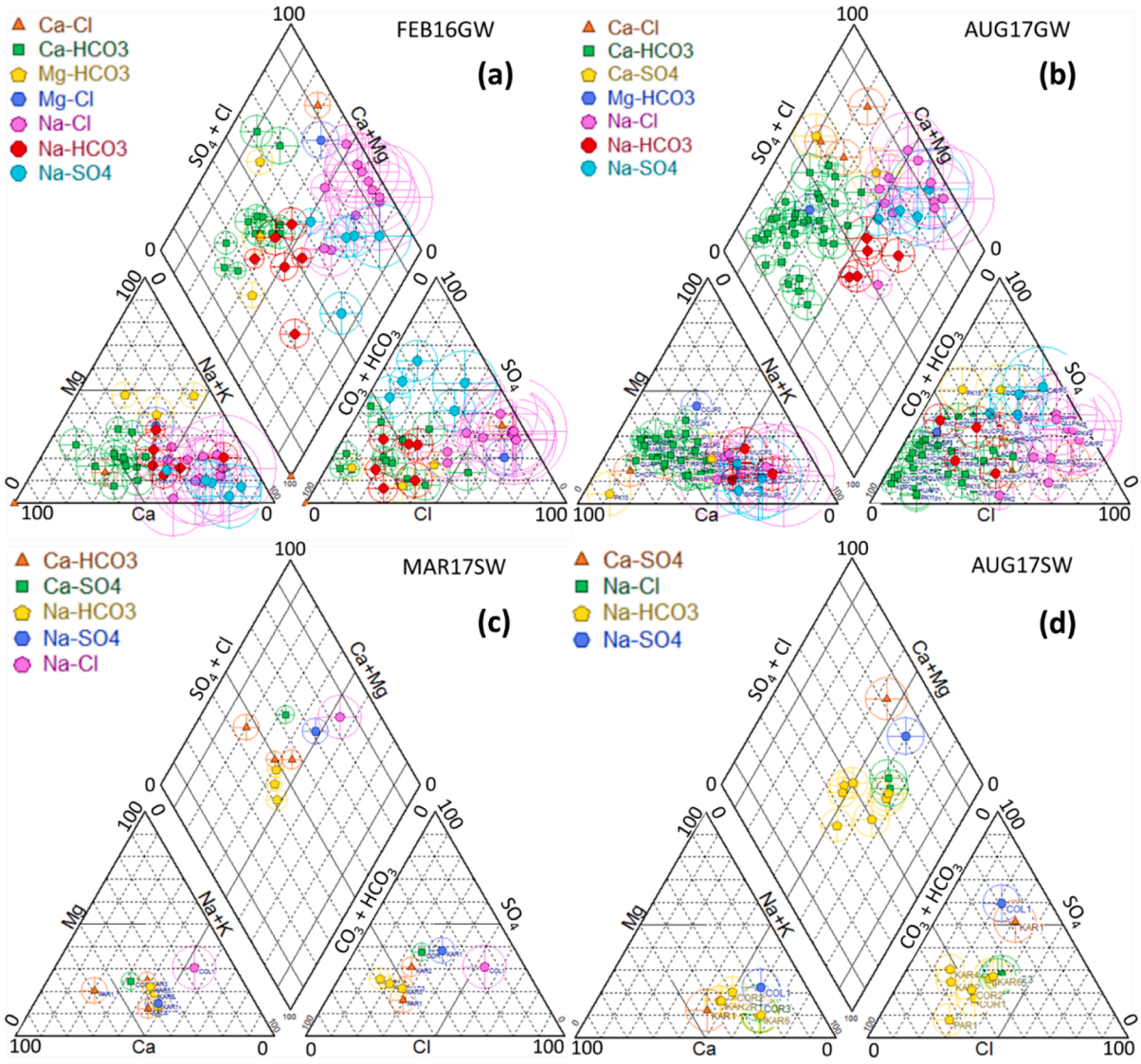

Fig. 7. Piper diagram showing major ions composition, water type and TDS values (open circle) in groundwater (GW): rainy season (February 2016) (a), and dry season (August 2017) (b). Surface water (SW): rainy season (MAR17) (c), and dry season (AUG17) (d).

Na^+ (Table 3).

4.3.3. Arsenic

Speciation of As indicates that the predominant oxidation state is As (V) with the range of 60–79 % of samples in RASE (GW and SW) and 70–100% in DRSE (GW and SW). The As concentration and other TEs in GW are shown in Fig. 6c, d.

The elevated concentration of As was noticed downstream of the basin (northwest area), in the wells with the most shallow phreatic level (mean in RASE: 0.6 m; mean in DRSE: 0.8 m), in a flood area (sediments of lacustrine origin), with a low slope (3.8%), within the north plain of Lacaya Cohana (LACP3) and Wilajahuira (WIP1) with 253.5 μg/L and 147 μg/L respectively in RASE whereas 288.5 μg/L and 233.3 μg/L respectively in DRSE (Fig. 8e, f, g, h). The mean value of As in this region (Cohana – Lacaya - Wilajahuira) is 156 μg/L in RASE and 190 μg/L in DRSE.

The slightly higher terrain around volcanic formations (Korila - Quiripujo - Lacaya - Chojasivi - Huacullani) has lower concentrations (RASE mean: 29 μg/L; DRSE mean: 22 μg/L). The general flow of water increases during the RASE, and it is assumed that this reduces the contact time between water and sediments, which would explain the trend of lower levels of As in high terrain during this season (Ormachea Muñoz et al., 2013).

In the wells near the Katari River of the central plain region, there are some sectors that have high concentrations of As such as Masaya (PK5: 81 μg/L; PK4: 109 μg/L) and Tircani (TIRP3: 86 μg/L). There is a predominant scenario for As-rich GW due to the presence of alluvial sediments (Bhattacharya et al., 2002a, 2002b). Especially in some wells located in the lowlands (PUJP1: 56 μg/L; IQUP1: 122 μg/L), there could be exchangeable As present in the sediments, which can be mobilized to GW due to increased salinity (Ormachea Muñoz et al., 2013) caused by evaporation. The wells situated in sedimentary rock formations, outside the north and northwest regions, have relatively low concentrations of As (mean: 21 μg/L), however, the threat to the population that uses this water for consumption still remains.

Arsenic concentrations increase by 16% in DRSE relative to RASE (Table 3). In general, in all sampling points of the study area, the As shows a lower correlation with iron (Fe) (R^2 = 0.5 in RASE) and no correlation with B, aluminum (Al), Mn, and other physicochemical parameters.

In general, all river water samples (SW) have a low concentration of As, except in the north plain region (flood delta) in DRSE, at the location of Cohana (COR1: 48 μg/L), Lacaya (COR2: 26 μg/L) and Calachaca (COR3: 25 μg/L) (Fig. 8e, f, g, h). The As concentration in COR1

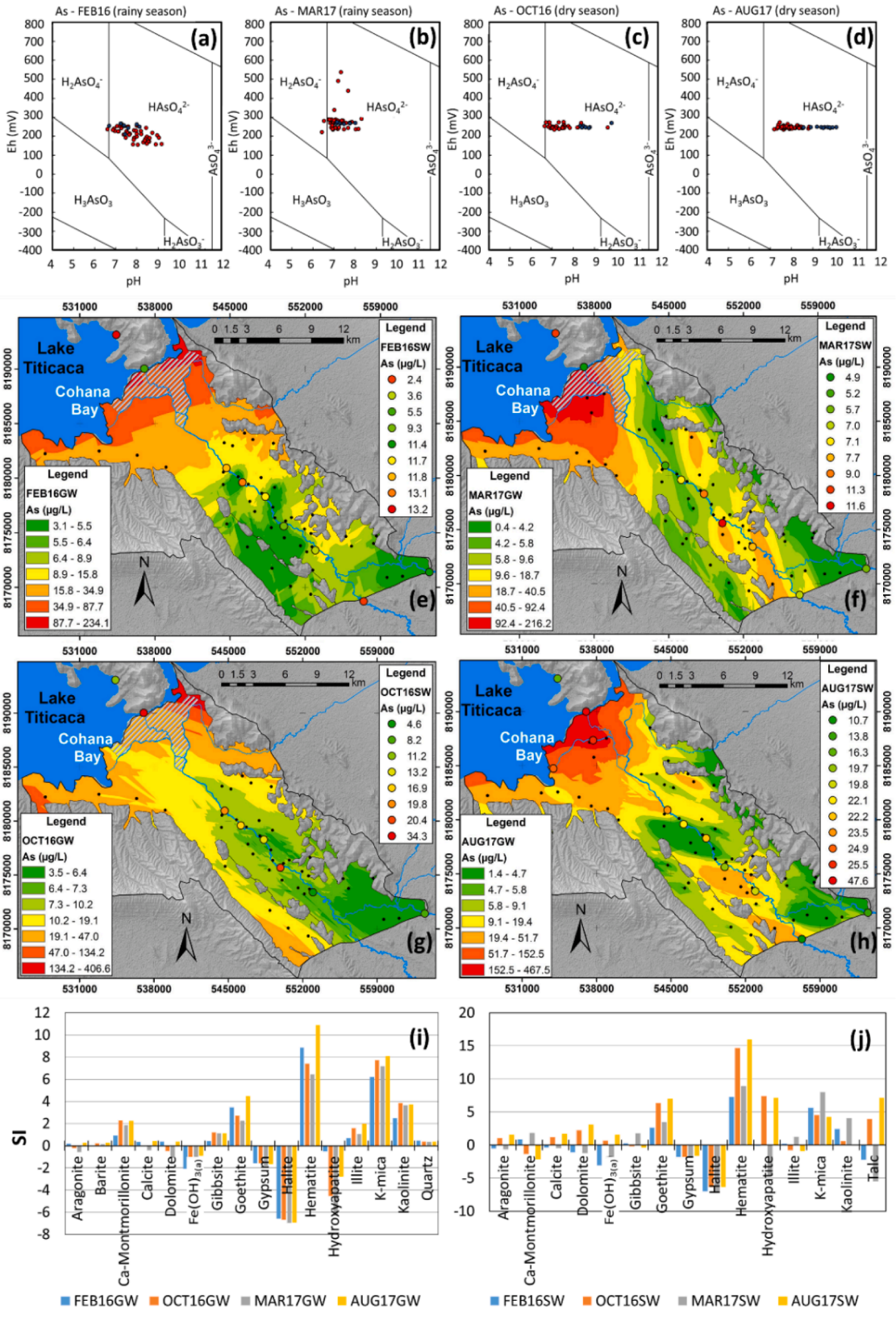

Fig. 8. The pH and Eh values for SW (blue) and GW (red) samples plotted in the Eh-pH diagram of aqueous As species in the water at 25 °C and 1 atm for the systems As-O–H (modified from Panagiotaras et al., 2012; Ticona, 2018). The rainy season (a, b) and dry season (c, d). Spatial and temporal variability of arsenic (As) in groundwater (GW) and flow surface water (SW) in rainy season FEB16 (e), MAR17 (f), and dry season: OCT16 (g), AUG17 (h). Mean values of the saturation indices (SI) for selected minerals: GW (i), and SW (j). (For interpretation of the references to color in this figure legend, the reader is referred to the web version of this article.)

(Cohana) increases in DRSE compared to RASE by 84% in 2016 and 90% in 2017.

The Katari River contains low levels of As in upstream of the basin, however, these levels increase along with the flow especially downstream of the basin in the same region where the wells have high concentrations of As (Cohana - Lacaya - Wilajahuira). The present results are strongly agreements with the findings related to the As concentration by evaporation as suggested by Banks et al., 2004, corroborated by the high salinity (considering the concentrations of Na^+ and Cl^-) in the same distance.

4.3.4. Trace elements

The B in GW is strongly correlated with Na^+ ($R^2 = 0.63$ in RASE; $R^2 = 0.70$ in DRSE) and Cl^- ($R^2 = 0.49$ in RASE; $R^2 = 0.52$ in DRSE). The B has highest concentrations in the southeastern of study area in the confluence area between Katari and Pallina rivers (mean: 573 μg/L; range: 284–1016 μg/L) and part of flat area (mean: 641 μg/L; range: 123–2473 μg/L) in DRSE. In RASE the B concentrations decrease by 20%.

The elevated Mn concentrations predominantly occurred in wells in central flat area (mean: 1159 μg/L; range: 0.6–6607 μg/L in RASE and mean: 1017 μg/L; range: 0.9–7259 μg/L in DRSE), close to the hills in the northeastern area (mean: 358 μg/L; range: 3–1370 μg/L in RASE and mean: 847 μg/L; range: 4–4725 μg/L in DRSE) and in the north plain (flood delta) (mean: 557 μg/L; range: 205–962 μg/L in RASE and mean: 782 μg/L; range: 199–1555 μg/L in DRSE). There is a decrease in Mn concentrations (around 30% except in the flat area) in RASE.

The strontium (Sr) concentrations (Table 3) were high in both seasons, however, there is a decrease in concentrations by 17% in RASE in relation to DRSE. This is especially observed in the wells in the central flat area (mean: 1389 μg/L; range: 82–4601 μg/L in RASE and mean: 1567 μg/L; range: 531–4746 μg/L in DRSE), in the southeastern of study area in the confluence area between Katari and Pallina rivers (mean: 963 μg/L; range: 385–1499 μg/L in RASE and mean: 1089 μg/L; range: 730–1532 μg/L in DRSE) and in the north plain (flood delta) (mean: 788 μg/L; range: 561–918 μg/L in RASE and mean: 943 μg/L; range: 573–1364 μg/L in DRSE). The Sr is strongly correlated with the ions Cl^- ($R^2 = 0.84$ in RASE; $R^2 = 0.82$ in DRSE), SO_4^{2-} ($R^2 = 0.75$ in RASE; $R^2 = 0.71$ in DRSE) and Na^+ ($R^2 = 0.73$ in RASE and DRSE).

Iron (Fe) concentration in GW increased about 59% in DRSE (Table 3). The Fe has high concentration in the north plain (flood delta) (mean: 547 μg/L; range: 25–1322 μg/L in RASE and mean: 655 μg/L; range: 27–1251 μg/L in DRSE). The concentration of lithium (Li) in GW has decrease of about 13% in DRSE (Table 3). The Li in GW is strongly correlated with Na^+ ($R^2 = 0.75$ in DRSE), Cl^- ($R^2 = 0.71$ in DRSE) and SO_4^{2-} ($R^2 = 0.67$ in DRSE).

The concentrations of silicon (Si), B, Sr, and Mn in SW samples are high during the DRSE (Table 3). The concentration of other TEs did not increase significantly in DRSE compared to RASE (Fig. 6g, h).

4.4. Hydrogeochemical calculations

The hydrochemical calculation with code PHREEQC considering the saturation indices (SI) indicated that the GW is supersaturated with respect to the Fe-oxide/hydroxide minerals such as goethite [α-FeOOH] and hematite [Fe_2O_3], and the Al minerals such as gibbsite [$Al(OH)_3$], K-mica [$KAl_3Si_3O_{10}(OH)_2$] and Kaolinite [$Al_2Si_2O_5(OH)_4$], suggesting precipitation of Fe (III) and Al (III) phases in GW. The SI for carbonate minerals such as calcite [$CaCO_3$], dolomite [$CaMg(CO_3)_2$] are more negative or at equilibrium, it could be suggesting that the chemistry of GW is controlled by precipitation and dissolution of carbonate minerals. The SI also revealed the dissolution of halite [NaCl] and gypsum [$CaSO_4{:}2H_2O$] minerals (Fig. 8i).

The calculation for species distribution in GW indicate that the predominant species is As (V) with 89% (FEB16), 66% (OCT16), 59% (MAR17) and 98% (AUG17), with different degree of protonation: $HAsO_4^{2-}$ (52% in FEB16, 50% in OCT16, 50% in MAR17 and 56% in AUG17) and $H_2AsO_4^-$ (9% in FEB16, 14% in OCT16, 19% in MAR17 and 4% in AUG17). While As (III) in GW is present as H_3AsO_3 (93% in FEB16, 96% in OCT16, 99% in MAR17 and 96% in AUG17). The predominant species in SW also is As (V) with 87% (FEB16), 100% (OCT16), 81% (MAR17) and 100% (AUG17). The As (V) in SW is present as $HAsO_4^{2-}$ (59% in FEB16, 48% in OCT16, 60% in MAR17 and 22% in AUG17) and $H_2AsO_4^-$ (13% in FEB16, 0.6% in OCT16, 12% in MAR17 and 0.1% in AUG17). The As (III) in SW is present as H_3AsO_3 (98% in FEB16, 76% in OCT16, 98% in MAR17 and 56% in AUG17).

4.5. Solid – Phase characterization

4.5.1. Lithological characteristics

The drilling and sediment sampling of the piezometers revealed high vertical variability in their characteristics and some differences between all sampling sites (17 piezometers). The study area has a recent Quaternary Formation corresponding to deposits of riverine and lacustrine origin, according to the information of the sediments at different levels taken during the drilling of the monitoring wells. These deposits of lacustrine origin could be formed by the silty clay and clay materials distributed in the extensive plain of the sector, the result of slow sedimentation events of lagoon processes.

The riverine deposits have varied sandy granulometry (fine, medium, and thick), a consolidated layer of 0.3 to 0.1 m is also evident, conformed by silt and clay. The variation in the lithology of the subsoil (lateral and in-depth) is shown in Fig. 10a, considering the lithological profiles of the piezometers parallel to the Katari riverbed. The piezometers were installed along an approximate length of 10 km, in a southeast-northwest direction, from the town of Pujri to the Catavi community, the piezometers that were used to elaborate the general lithological profile are PK1, PK2, PK6, PK8, and PK10 (Fig. 10a).

The lithological profile shows several layers of lacustrine origin to riverine-lacustrine with intercalations of fine material such as clay, silt, and organic matter with the sand horizons between thin, medium, and thick. The depth of the profiles reached in a range of 3 to 5 m, where the first sedimentation layer is composed of medium to thick grain sand, with a thickness between 1.3 and 5 m of depth. Besides, some clay layers are observed in a range of 0.4 to 0.9 m thick. The overlying layer is composed of a mixture of a varied proportion of clay and brown consolidated silt, generating a thickness that decreases from 0.3 to 0.1 m; so that decrease in depth from 2 to 1.4 and 2.3 m is also observed along with the profile (Fig. 10b, c, d, e). The upper contiguous layer is composed of slow deposition lacustrine material, such as yellow clays (portions) and black with an organic matter where its thickness changes from 0.85 m at the beginning of the profile to 0.6 m, and then reaches its thickness again at the finish the same 0.85 m.

The surface layer is formed by silty clay deposits constituting a thickness of 1.8 to 2.4 m along with the profile. The lithological record of the superficial perforations, and those of the lithology in the communal wells of the area, allow indicating at the regional level the existence of hydrogeological units constituted by lacustrine and riverine materials of the geological formation of the quaternary.

4.6. Hydrology

4.6.1. Aquifer units

The phreatic level in piezometers and communal wells is below the impermeable and semi-impermeable layers of silt and clays (Fig. 4a, b, c, d). In other shallow wells, it could be assumed that they are free aquifers (aquifer containing unconfined groundwater that has a water table and an unsaturated zone) (UN, 2019), it would not be strange if there was also the presence of semi-confined aquifers, and this can only be corroborated by a more detailed geophysical and hydrogeological analysis.

4.6.2. Groundwater flow direction

In order to estimate the direction of GW flow-through static levels, the topographic levels of the region, both piezometers and communal wells in the area (at ground level) were considered, making measurements to the millimeter this due to the smooth slope of the plain (Fig. 9). The hydraulic load and the hydraulic gradient are calculated with the elevation information (topographic levels) and static levels recorded during GW collection.

An equipotential map of the GW level is drawn up that graphically represents the direction of the GW in the direction from southeast to northwest (SE-NW), based on the topographic map, the static levels, and the hydraulic load. The GW course presents a similar trend to the surface watercourse and the topography of the area, with gentle slope changes in the plain (Fig. 9).

4.6.3. Hydrogeological signature of study

According to the first evaluation carried out in the hydrogeological study, it was possible to demonstrate the formation of a shallow aquifer unit, which was formed by the debris of medium to coarse sand with a varying thickness according to depth reached from 0.5 to 1.3 m. The direction of GW flows still under evaluation and indicates that it flows from southeast to northwest, showing sectors where GW flows to the river in the towns of Chacalleta and Pujri, and in the lower area of the plain, the river flows into the GW (Fig. 9). It was not possible to clearly define the recharge zones that allow identifying the origin of the GW in the study area. The analysis and interpretation of environmental isotopes are required. It is also considered important to be able to obtain information on the hydraulic parameters of the deep aquifer units.

4.7. Geochemical characteristics of sediments

4.7.1. Elemental characteristics of core sediments of piezometers

The mean values of the total extraction of As in each piezometer are presented in Table 4 for sediment samples of LKB in order of southeast to northwest (Fig. 9). In a layer of piezometers PK6 and PK12, high As levels were identified, at depth of 3 m below the ground surface, containing 62.9 and 84.8 mg/kg respectively (Fig. 10f). The existence of As_{total} were found in PK2 (2.2 m: 24.5 mg/kg; 3 m: 26.4 mg/kg), PK10 (2.7 m: 25.8 mg/kg), PK13 (2 m: 24.6 mg/kg; 5 m: 28 mg/kg), PK14 (3 m: 29.6 mg/kg), PK15 (3 m: 27.9 mg/kg), PK16 (2 m: 20.3 mg/kg) and PK19 (2.5 m: 23.1 mg/kg) which represents a tendency to increase the As_{total} content with depth. The mean content of As and TEs (Fe, Al, Sb, B) shows a low correlation (As: $R^2 = 0.46$).

The mean values of Fe and Al in all piezometers were found ranged between 18.6 and 27.1 g/kg and 9.6–24.6 g/kg respectively, where Mn content was observed lower as 0.3–1.2 g/kg. There is a tendency to

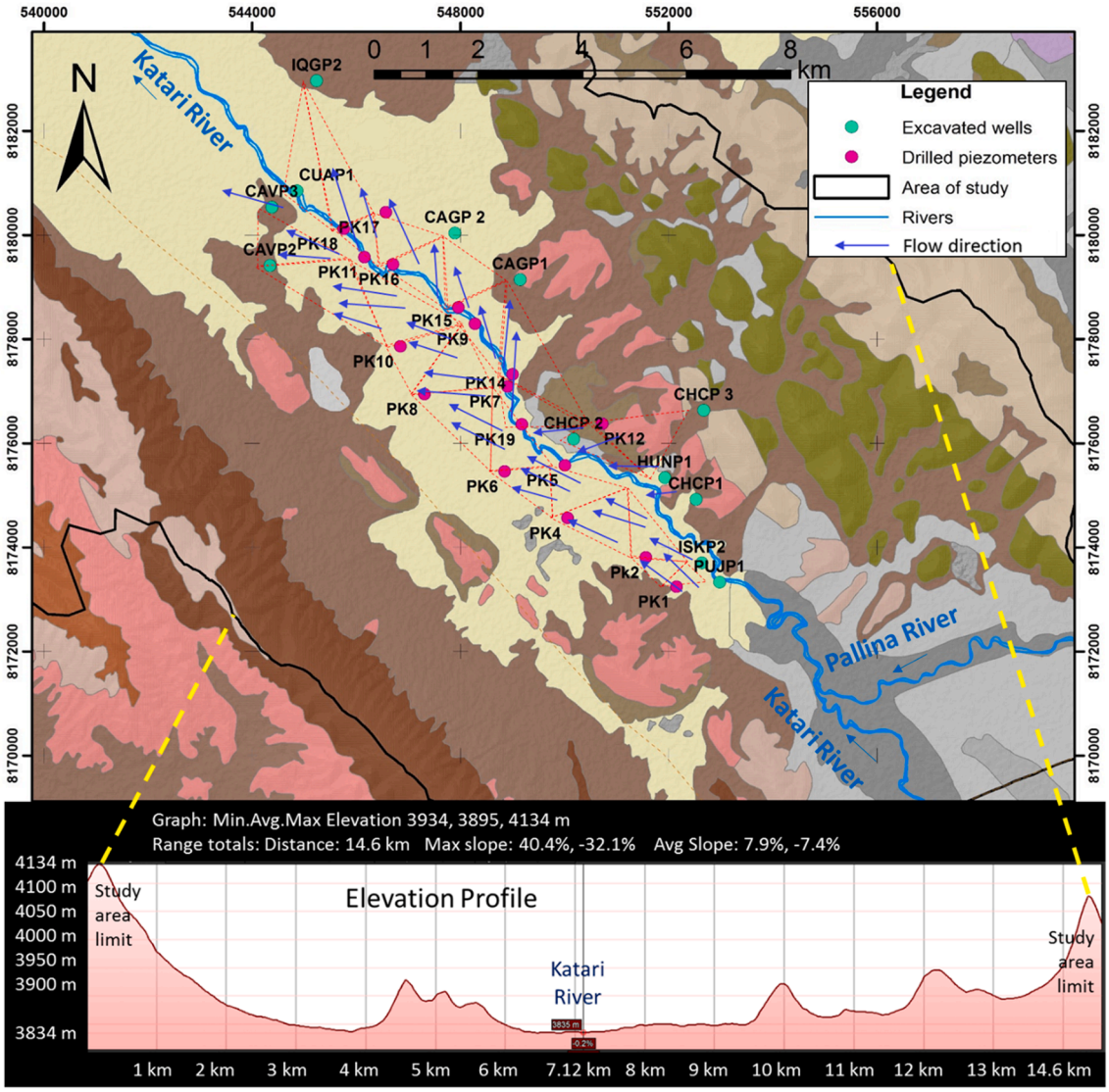

Fig. 9. Geographical location of piezometers and wells, groundwater flow direction and cross elevation profile (Google Earth Pro, 2019).

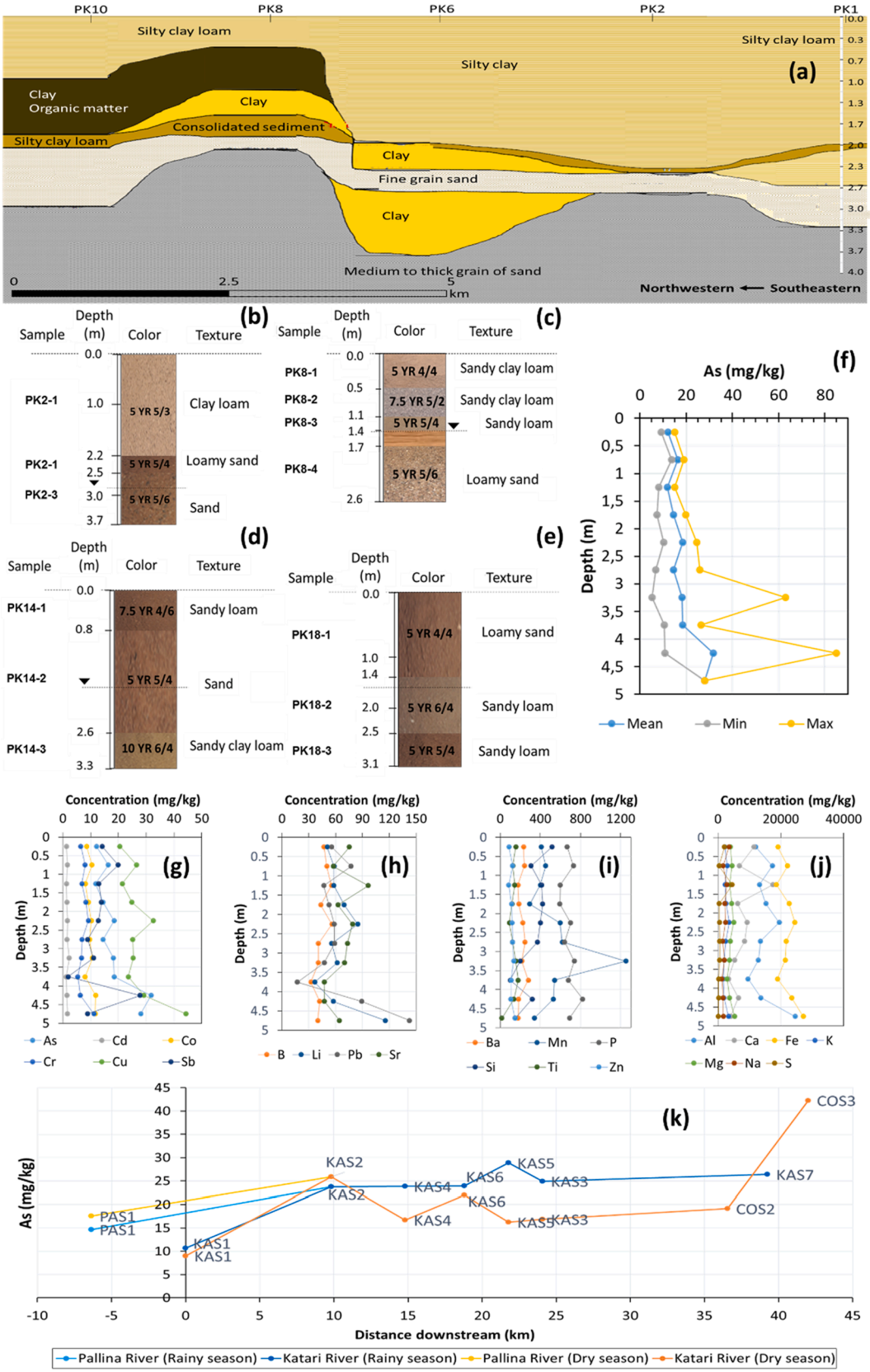

Fig. 10. Distribution for lithological profiles (plain area) (a). Color and texture of piezometers: PK2 (b), PK8 (c), PK14 (d) and PK18 (e). Arsenic content from the total extraction of the core sediments from the piezometers (mean values) (f). Trace elements content from total extraction of the core sediments from the piezometers (mean values) (g, h, i, j). Seasonal variations of As content from total extraction of the sediments corresponds to Pallina and Katari rivers (k).

Table 4
Total extraction of arsenic in core sediment samples from piezometers in Lower Katari Basin (LKB).

Katari River (LKB)					
Left side (flat area)			Right side (flat area)		
Code	Place	As (mean)	Code	Place	As (mean)
		mg/kg			mg/kg
PK1	Iskacaspa	10.4	PK12	Chacalleta	37.6
PK2	Iskacaspa	23.2	PK19	Chacalleta	15.7
PK3	Iskacaspa	7.5	PK13	Chacalleta	26.3
PK4	Masaya	9.5	PK14	Caje	19.8
PK5	Masaya	9.7	PK15	Caje	20
PK6	Masaya	31.1	PK16	Mucuña	13.4
PK7	Caleria	11.7	PK17	Mucuña	11.1
PK8	Caleria	13.6	PK18	Coachijo	13.7
PK9	Caleria	11.2			
PK10	Caleria	20.3			
PK11	Catavi	15			

increase the concentration of these elements with depth (Fig. 10g, h, i, j). A significant difference in sulfur (S) content was observed in PK1 (mean: 118.9 mg/kg) and PK8 (mean: 7278.0 mg/kg). In PK8, elevated S concentrations were found at depths of 0.5–3 m. In reducing condition of the sediments, As could be bound to sulphides (Ormachea Muñoz et al., 2013). The elevated concentration of calcium (Ca) was found in PK11 (11.1 g/kg), PK3 (12.8 g/kg), PK7 (13.2 g/kg), PK18 (15.7 g/kg), and PK8 (22.7 g/kg), at depths of 0.5–3 m, however, a slight decreasing trend of Ca content was observed with depth in the shallow sediments.

4.7.2. Elemental characteristics of river sediments

In Pallina River in PAS1 and at the confluence between the Pallina and Katari rivers in KAS2, there is an increase in As concentration in DRSE from 14.6 to 17.5 mg/kg (19.6%) and from 23.7 to 25.9 mg/kg (9%), respectively (Fig. 10*k*). On the contrary, there is an increase in As concentration in Katari River in RASE by 16% in KAS1, 32% in KAS3, 30% in KAS4, 44% in KAS5, and 8% in KAS6 (Fig. 10*k*). The highest As content was found in Katari River in the northwest of the study area in the Lacaya region (COS3) 42.3 mg/kg, near CB (Fig. 2).

The concentration of Fe in the sediments varied with in a range of 19.8–22.1 g/kg in RASE and 18.2–26.9 g/kg in DRSE, where 4% of increased concentrations was observed in DRSE. The range of Al concentration varied between 9.7–15.2 g/kg and 5.9–15.4 g/kg in the RASE and DRSE respectively. The comparison of the content of the other TEs such as Mn (RASE range: 283.6–492 mg/kg; DRSE range: 270.1–474.4 mg/kg), Zn (RASE range: 90.8–212.8 mg/kg; DRSE range: 74.7–491.1 mg/kg), Si (RASE range: 78.5–273.5 mg/kg; DRSE range: 98–170.7 mg/kg), B (RASE range: 43.4–64.1 mg/kg; DRSE range: 50.2–88.9 mg/kg), Sb (RASE range: 3.1–4.9 mg/kg; DRSE range: 3.4–60.3 mg/kg) and Li (RASE range: 48.6–67.9 mg/kg; DRSE range: 34.3–92.4 mg/kg) were variable, but no trends were observed.

4.7.3. Sequential extraction of as in core sediments of piezometers

The sequential extraction procedure of the BCR method (Ure et al., 1993) allowed to determine the distribution of As; and among the different geochemical fractions (F1, F2, F3, and F4), which reflected the relative proportions of As transported by different chemical mechanisms (Fig. 11).

The As-rich layers found from highest to lowest through the sequential extraction in first layer (0.1–1.5 m) as F4 (range: 6.4–33.4 mg/kg), F2 (range: 0.3–2.6 mg/kg), F1 (range: 0.2–1.7 mg/kg) and F3 (range: 0.1–0.9 mg/kg). In the second layer (1.5–2.5 m), it (from highest to lowest) exhibited as F4 (range: 11.7–94 mg/kg), F2 (range: 0.03–5.7 mg/kg), F1 (range: 0.1–5.1 mg/kg) and F3 (range: 0.2–1.2 mg/kg). In the third layer (2.4–3.2 m), it (from highest to lowest) was noticed as F4 (range: 10.2–38.7 mg/kg), F2 (range: 0.5–3.6 mg/kg), F1 (range: 0.2–1.9 mg/kg) and F3 (range: 0.3–1 mg/kg). Finally, the last layer (2.5–3.3 m), it (from highest to lowest) was observed as F4 (range: 12.1–16.4 mg/kg), F2 (range: 1.3–1.6 mg/kg), F1 (range: 0.5–1 mg/kg) and F3 (range: 0.3–0.4 mg/kg).

In all cases, the concentration of As was highest in the F4 (residual fraction), followed by F2 (reducible fraction), F1 (exchangeable fraction) and F3 (oxidizable). The concentrations of As extracted are much higher in layers 2 and 3 (Table 5). In general, being the largest residual fraction (approximately 84%), the As is associated with primary and secondary minerals, it probably does not dissolve under natural conditions (Mäkelä et al., 2011), this indicates that the As has reduced mobility (low release of As by sediment) (F4). The reducible fraction of As is approximately 9%, which this indicates the As is associated with oxides of Mn and Fe, and forms normally known as sinks of TEs in a surface environment (Silveti et al., 2013) (F2). In 5% of the extractions, the As is found exchangeable form, it could be released by ion exchange processes or co-precipitated with carbonates, this form would be the most readily available (Gleyzes et al., 2002) (F1). Finally, only 2% of the extractions are in the oxidizable form (sulfides); in this form, the As is not considered bioavailable (Filgueiras et al., 2002) (F3) (Fig. 11).

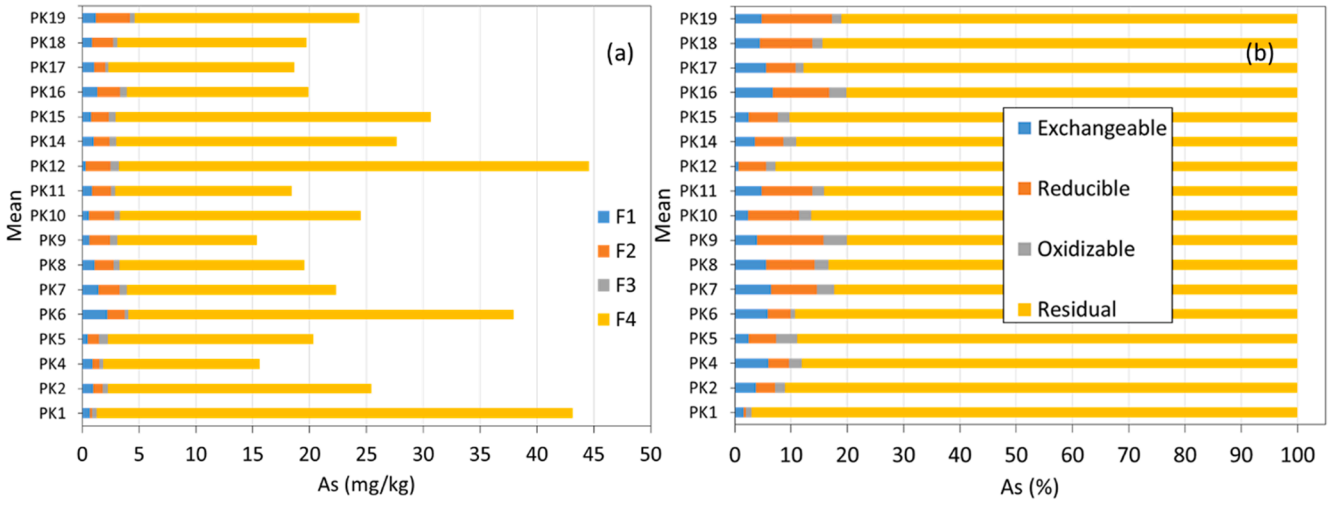

Fig. 11. Mean values of sequential extraction of As from each sediment by piezometer in mg/kg (a) and % (b).

Table 5
Mean values of sequential extraction BCR (Community Bureau of Reference) by levels and fractions.

Mean values				
	F1	F2	F3	F4
Level	Exchangeable	Reducible	Oxidizable	Residual
	%	%	%	%
First (n = 17)	4.7	9.4	2.9	83.1
Second (n = 17)	4.3	6.5	2.3	86.9
Third (n = 14)	4.5	7.6	2.2	85.8
Fourth (n = 3)	4.9	9.0	2.1	84.1
	mg/kg	mg/kg	mg/kg	mg/kg
First (n = 17)	0.8	1.5	0.5	15.2
Second (n = 17)	1.2	1.7	0.6	29.8
Third (n = 14)	1.0	1.7	0.5	21.7
Fourth (n = 3)	0.8	1.5	0.3	14.1

5. Discussions

5.1. Sources of arsenic

The concentrations of As in the study area shows a progression of As enrichment, however, these are located in specific regions such as flood area, which indicates the distribution of As is not homogeneous in the basin. The northern region (flood plain area), specifically the flat region, has the highest As concentration, this indicates that sediments are the most important sources of As.

The concentrations of As in sediments are slightly higher than the global mean estimated 1–5 mg/kg (Bhattacharya et al., 2002a, 2002b; Ravenscroft et al., 2009; Ormachea Muñoz et al., 2013), because alluvial sediments are the predominant scenario for GW enriched in As such as in many places of the world (Bhattacharya et al., 2002a, 2002b).

The As concentrations in the sediments are varied according to the depth, as the second (2–3.5 m) and the third level (3.5–4.5 m) where have clays, silts, and fine sands, and which have sediments of lacustrine origin (As: 63–84 mg/kg maximum values). There are considerable variations of As concentration in between/or different strata, which leads to indicate a high spatial variety in the characteristics of the sediments.

The high variation in As concentrations could be explained as a consequence of the alluvial processes from the Paleo lakes and the subsequent wind processes that would have redistributed the material over the entire Altiplano, making the sediments more heterogeneous (Ormachea Muñoz et al. 2013). The evaporites (sedimentary rocks that are formed by crystallization of dissolved salts in lakes) intermingle with the sediments found in places that have high As contents, which makes their distribution irregular (Banks et al, 2004).

The direct effect of volcanic rocks on water quality in the northwest region near Lake Titicaca is limited, since As concentrations are lower compared to those in the northern region where lacustrine sediments predominate. Volcanic rock weathering, despite its moderate As content, is considered in many studies as an important source of As (Smedley and Kinniburgh, 2002; Banks et al., 2004; Schnoor, 1996; Ormachea Muñoz et al., 2013, 2016; Tapia and Audry, 2013). Higher values of pH (>8.5) and Na^+ indicate these rocks (Smedley and Kinniburgh, 2002) would affect that GW.

The Tiwanaku, Coniri and Kollu-Kollu geological formations of the Tertiary and Quaternary age (Martínez et al., 2007) represents in the study area, which has a significant influence on the general water chemistry in particular of the northwestern region. The As and B are elements are existed in volcanic deposits (northwest region), exhibiting a correlation (EC *vs* As: $R^2 = 0.36$; EC *vs* B: $R^2 = 0.65$) with the salinity of GW. Due to this characteristic, they could be expected to persist in SW and accumulate in GW (Ormachea Muñoz et al., 2013).

The salinity of the northern plain in a semi-arid climate, the evaporation could mobilize some types of exchangeable As present towards the GW. On the contrary, the low concentrations of As in the central and southern plains of the study area, having waters enrichment in Ca^{2+} and HCO_3^-, could indicate that As is linked to $CaCO_3$ minerals that are insoluble, especially at high pH (Stollenwerk et al., 2002).

5.2. Sediment-water interaction

Sediments consist of a dominant texture class clay-sandy-loam and have good drainage capacity and probably good aeration. The amount of extracted As in different depth levels has a certain correlation with the type of sediment material, the second (1.5–2.5 m), and the third (2.5–3.2 m) level, which are composed of finer materials (sandy-clay-loam). This would reflect the greater weathering of fine sediments due to their greater reactive surface area (Gustafsson et al., 2006; Ormachea Muñoz et al., 2013).

Since, most of the As is found in the residual fraction (F4 = 84%) in the sediments of the central region of the plain, the role of refractory primary minerals (Fe, Al) is essential. Although the As has reduced mobility in the sediments, its high concentration indicates that in the long term they could be a very important source of As contamination for the environment, being able to develop the dissolution of minerals with high As content.

High pH values together with the oxic characteristic of the terrain are conducive to the increase in As concentrations (Smedley and Kinniburgh, 2002; Bhattacharya et al., 2006), due to the decrease in As adsorption to the oxides and hydroxides of Fe and Al, which vary according to the pH (Appelo and Postma, 2005). That is why; even a small increase in pH could generate a significant increase in As concentration in GW. This is evidenced in the pH values in the northern plain (RASE mean: pH = 7.3; DRSE mean pH = 7.9). The adsorption of As to oxides and hydroxides of Fe and Al decreases under oxidizing condition, in addition to high pH values, with a reduction in adsorption and stability of AsO_4^{3-} (Stollenwerk et al., 2002).

The importance of carbonates in As levels in GW is not entirely clear, since in the geochemical modeling the SI found reveal that GW is unsaturated or in equilibrium with respect to calcite in some wells. Since it is known that the adsorption of As in calcite or clay minerals could be one of the most important As immobilization processes in areas with a pH range 7–9 (Stollenwerk et al., 2002; Romero et al., 2004; Ormachea Muñoz et al., 2013). Another study indicates that carbonates have a negative effect on the adsorption of As to Fe oxides (Claesson and Fagerberg, 2003; Stollenwerk et al., 2002; Ormachea Muñoz et al., 2013; Ahmad et al., 2019).

The interchangeable fraction (F1 = 5%) in the region of the central and southern plains could indicate that the As in sediments can be better mobilized at higher pH, however, being low (only 5%) in relation to the other fractions suggests that the pH has a low impact on the release of As in this region. The adsorption of As due to the oxides and hydroxides of Fe, Al, and Mn which is one of the most studied processes regarding the mobility of As in natural waters (Bhattacharya et al., 2006; Van Genuchten and Ahmad, 2020; Ahmad et al., 2019), represents the second most important fraction of the study (F2 = 9%).

The insignificant correlation was exhibited between As and Fe concentrations in GW samples throughout the region (R^2 = 0.27–0.52) except in the northern plain region (R^2 = 0.93–0.94). The lack of a correlation between these two elements indicates that the reducing dissolution is not important in the region, corroborated with the values of E_h (slightly oxidizing medium). Under reducing conditions, the oxides of Fe (III) with adsorbed As are dissolved, Fe and releases As (Gustafsson et al., 2006), and this reductive dissolution is a common cause of the high concentration of As (Bhattacharya et al., 2006). This process explains the good correlation between As and Fe (R^2 = 0.93–0.94) in the northern plain region.

Geochemical modeling indicates the probable precipitation of oxides

and hydroxides of Fe and Al in the study area with the exception of the north and northeast region, which confirms the As adsorbents. There are several minerals that according to the SI would be responsible for the low As values, such as hematite [Fe_2O_3], goethite [α-FeOOH], gibbsite [Al $(OH)_3$], K-mica [$KAl_3Si_3O_{10}(OH)_2$], and kaolinite [$Al_2Si_2O_5(OH)_4$].

Possible evaporation conditions could be an important factor for the high concentration of As in GW (Bhattacharya et al., 2006), considering that the GW levels are shallow in the northern region (0.6–0.8 m) and northeast (1.1–0.9) of the study area. The Si is an important element that could be competing for adsorption spaces in minerals, because it has significant concentrations in the north (8.4–8 mg/L) and northwest (13.1–12.5 mg/L) regions, where As concentrations are also high. It is known that high Si values (10 mg/L) and an elevated pH could decrease As adsorption (Stollenwerk et al., 2002; Davis et al., 2001; Ormachea Muñoz et al., 2013).

6. Conclusions

The lack of good quality water (according to NB-512 and WHO guidelines) for consumption in the northwest, north, east, and the right side of Katari River in the plain area is due to the low rainfall (semi-arid climate) and high salinity (salt evaporation). The water bodies in LKB are affected by the elevated presence of As, B, Mn, and NO_3^-, this problem remains despite the fact that the SW presents dilution in its salt and mineral contents after the confluence of Pallina and Katari rivers. The SW does not represent a possible source of drinking water due to the negative effect of wastewater (Pallina River) and its entire load (solids and liquids) along the Katari River.

The large temporal variation in the amounts of water causes a direct action on GW and a larger scale on SW. The drag material coming from the wastewater represents a significant negative health impact for LKB and in particular for the populations of the lower part (Wilajahuira, Lacaya, Pampa Cohana). The general trend in the direction of GW flow is from southeast to northwest, showing sectors with probable interaction between SW and GW.

The highest concentrations of As in GW are found downstream of the basin (northwest area) and could be associated with alluvial sediments enriched with As. It was observed that due to the low slope (3.8%) the GW would have a slow movement and along with the large surface area of fine-grained sediments, would be facilitating the release of As. In RASE, there is a decrease in As concentrations because, as the flow of water increases, the contact time between water and sediment is reduced. The SW with somewhat higher concentrations of As is found downstream of the basin, which is enriched the concentration of As, due to evaporation, possibly.

The geological characteristics of LKB generate a great spatial variability of As, due to the presence of evaporites that are distributed unevenly in the sediments. In the region where volcanic formations exist although the concentrations are lower compared to the northern plain, it is still harmful to health. Another important phenomenon considers the As, B and Li present in the SW that would be accumulating in the GW and the interchangeable As in the lowlands could be mobilized to the GW due to the increase in salinity (semi-arid climate and evaporation of salts), especially in the plain region.

Sequential extraction of sediments and geochemical modeling indicates that As is associated with the oxides and hydroxides of Fe and Al, which are probably the most important adsorbents of As in the sediments. The low mobility of As in the central and southern region of the basin would be due to calcium carbonates (e.g. calcite). Although the mobility of As in the sediments of these areas is reduced, its high concentration indicates that in the long term it could become a great source of water contamination.

For future studies in the area, it is recommended to model surface water flows and quality by applying QUAL2KW or other surface water modeling software.

The Sustainable Development Goal 6 (SDG 6) was established by the United Nations General Assembly in 2015, which fundamentally deals with " Ensure availability and sustainable management of water and sanitation for all". This study promotes technological empowerment of people (rural populations of the study area) to implement the SDGs.

As a consequence of this study, a monitoring network of water bodies and sediments was established, which is very useful to evaluate the quality and quantity of the water in the shallow aquifers and the surrounding rivers. The knowledge generated now serves to suggest possible mitigation options that can be adopted by local communities, as well as other interesting parties in mitigation of water pollution (decision-makers in water management policies such as the Ministry of Water, municipal governments, and water committees). The identification of the problem (As contamination and other trace metals), the current deteriorated state of drinking water in some regions of the basin was evidenced. Areas with major suitability for use as a source of drinking water are proposed, taking into account the early quantification of As contamination, as well as the identification of its natural sources and the processes of mobilization and environmental availability.

Declaration of Competing Interest

The authors declare that they have no known competing financial interests or personal relationships that could have appeared to influence the work reported in this paper.

Acknowledgements

The financial support of this research by the Swedish International Development Cooperation Agency (Sida Contribution: 75000553) is gratefully acknowledged. We would like to thank the chemist researchers Raúl Quispe and Irma Ticona at Instituto de Investigaciones Químicas, Universidad Mayor de San Andrés for anion and sediment analysis. We extend our sincere appreciation to researchers Magali Cori, Jhovana Ticona, Edson Chalco, Edwin Callisaya, Romel Aruquipa and Efrain Blanco for their fieldwork, as well as Hermenegildo Fernández and Rubén Choque for their field support. Additionally, we thank Magnus Mörth, at the Department of Geological Sciences, Stockholm University, for the trace elements analysis, and hydrologist technicians Franklin Mujica, Wilder Ramírez and David Terrazas at Servicio Nacional de Meteorología e Hidrología - Bolivia for flow measurements of surface water.

References

Ahmad, A., Bhattacharya, P., 2019. Arsenic in Drinking Water: Is 10 μg/L a Safe Limit? Curr. Pollut. Rep. 5 (1), 1–3.

Ahmad, A., Heijnen, L., Battaglia-Brunet, F., Oorthuizen, W., Pieterse, B., Bhattacharya, P., van der Wal, A., 2020. Mobility and redox transformation of arsenic during treatment of artificially recharged groundwater for drinking water production. Water Res., 115826

Ahmad, A., Rutten, S., Eikelboom, M., de Waal, L., Bruning, H., Bhattacharya, P., van der Wal, B., 2019. Impact of phosphate, silicate and natural organic matter on the size of Fe(III) precipitates and arsenate co-precipitation efficiency in calcium containing water. Sep. Purif. Technol. 235.

Ahmad, A., van der Wal, B., Bhattacharya, P., van Genuchten, C.M., 2019. Characteristics of Fe and Mn bearing precipitates generated by Fe(II) and Mn(II) co-oxidation with O2, MnO4 and HOCl in the presence of groundwater ions. Water Res. 161, 505–516.

Ahmad, A., van der Wens, P., Baken, K., de Waal, L., Bhattacharya, P., Stuyfzand, P., 2020. Arsenic reduction to <1 μg/L in Dutch drinking water. Environ. Int. 134, 105253.

ALT (Autoridad Binacional del Sistema Hídrico TDPS), 2017. Observatorio Binacional Titicaca V.01. ⟨http://www.observatoriotiticaca.org/web/⟩.

ALT (Autoridad Binacional del Sistema Hídrico TDPS), 2005. Diagnóstico del nivel de contaminación de los recursos hídricos del Lago Titicaca. ⟨http://www.alt-perubolivia.org/web_lago/WEB_LT/Finales/2_carac_fisicas/carac.htm⟩.

Appelo, C.A.J., Postma, D., 2005. Geochemistry, groundwater and pollution, 2nd Edition. Balkema, A.A, p. 649.

Archundia, D., Duwig, C., Lehembre, F., Chiron, S., Morel, M.-C., Prado, B., Bourdat-Deschamps, M., Vince, E., Flores Aviles, G., Martins, J.M.F., 2016. Antibiotic pollution in the Katari subcatchment of the Titicaca Lake: Major transformation products and occurrence of resistance genes. Sci. Total Environ. 576, 671–682.

Archundia, D., Duwig, C., Spadini, L., Uzu, G., Guedron, S., Morel, M., Cortez, R., Ramos, O., Chincheros, Martins, J.M.F., 2017. How uncontrolled urban expansion increases the contamination of the Titicaca Lake Basin (El Alto, La Paz, Bolivia). Water Air Soil Pollut. 228, 44.

Aullón Alcaine, A., Schulz, C., Bundschuh, J., Jacks, G., Thunvik, R., Gustafsson, J.P., Mörth, C.M., Sracek, O., Ahmad, A., Bhattacharya, P., 2020. Hydrogeochemical controls on the mobility of arsenic, fluoride and other geogenic co-contaminants in the shallow aquifers of northeastern La Pampa Province in Argentina. Sci. Total Environ. https://doi.org/10.1016/j.scitotenv.2020.136671.

Avila Sandoval, C., Júnez Ferreira, H., González Trinidad, J., Bautista Capetillo, C., Pacheco Guerrero, A., Olmos Trujillo, E., 2018. Spatio-Temporal Analysis of Natural and Anthropogenic Arsenic Sources in Groundwater Flow Systems. Int. J. Environ. Res. Public Health. https://doi.org/10.3390/ijerph15112374.

Ayotte, J., Belaval, M., Olson, S., Burow, K., Flanagan, S., Hinkle, S., Lindsey, B., 2015. Factors affecting temporal variability of arsenic in groundwater used for drinking water supply in the United States. Sci. Total Environ. https://doi.org/10.1016/j.scitotenv.2014.02.057.

Banks, D., Markland, H., Smith, P.V., Mendez, C., Rodriguez, J., Huerta, A., Sæther, O.M., 2004. Distribution, salinity and pH dependence of elements in surface waters of the catchment areas of the Salars of Coipasa and Uyuni, Bolivian Altiplano. J. Geochem. Explor. 84, 141–166.

Bhattacharya, P., Chatterjee, D., Jacks, G., 1997. Occurrence of arsenic contaminated groundwater in alluvial aquifers from Delta Plains, Eastern India: options for safe drinking water supply. Int. J. Water Resour. Manag. 13 (1), 79–92.

Bhattacharya, P., Jacks, G., Ahmed, K.M., Khan, A.A., Routh, J., 2002a. Arsenic in groundwater of the Bengal Delta Plain Aquifers in Bangladesh. Bull. Environ. Contam. Toxicol. 69 (4), 538–545.

Bhattacharya, P., Frisbie, S.H., Smith, E., Naidu, R., Jacks, G., Sarkar, B., 2002b. Arsenic in the environment: a global perspective. In: Sarkar, B. (Ed.), Handbook of heavy Metals in the Environment. Marcell Dekker Inc., New York, pp. 147–215.

Bhattacharya, P., Claesson, M., Bundschuh, J., Sracek, O., Fagerberg, J., Jacks, G., Martin, R.A., Storniolo, A.R., Thir, J.M., 2006. Distribution and mobility of arsenic in the Río Dulce alluvial aquifers in Santiago del Estero province, Argentina. Sci. Total Environ. 358 (2006), 97–120.

Bhattacharya, P., Welch, A.H., Stollenwerk, K.G., McLaughlin, M.J., Bundschuh, J., Panaullah, G., 2007. Arsenic in the environment: biology and chemistry. Sci. Total Environ. 379, 109–120.

Bhattacharya, P., Hossain, M., Rahman, S.N., Robinson, C., Nath, B., Rahman, M., Islam, M.M., von Brömssen, M., Ahmed, K.M., Jacks, G., Chowdhury, D., Rahman, M., Jakariya, M., Persson, L.Å., Vahter, M., 2011. Temporal and seasonal variability of arsenic in drinking water wells in Matlab, Southeastern Bangladesh: A preliminary evaluation on the basis of a 4 year study. J. Environ. Sci. Health, Part A 46 (11), 1177–1184.

Black, C.A., 1965. Methods of soil analysis. Part 1. American society of Agronomy, Madison, Winsconsin. USA, p. 1572.

Bundschuh, J., Pérez Carrera, A., Litter, M., 2008. Distribución del arsénico en las regiones Ibérica e Iberoamericana (Arsenic distribution in Ibero & Iberoamerican regions; in Spanish). Editorial CYTED, Buenos Aires, Argentina.

Bundschuh, J., Armienta, M.A., Birkle, P., Bhattacharya, P., Matschullat, J., Mukherjee, A.B. (Eds.), 2009. Natural Arsenic in Groundwaters of Latin America. Taylor & Francis Group, London, pp. 3–15.

Bundschuh, J., Litter, M., Ciminelli, V., Morgada, M.E., Cornejo, L., Garrido Hoyos, S., Hoinkis, J., Alarcón-Herrera, M.T., Armienta, M.A., Bhattacharya, P., 2010. Emerging mitigation needs and sustainable options for solving the arsenic problems of rural and isolated urban areas in Latin America — a critical analysis. Water Res. 44 (19), 5328–5345.

Bundschuh, J., Litter, M.I., Parvez, F., Román-Ross, G., Nicolli, H.B., Jiin-Shuh, J., Chen-Wuing, L., López, D., Armienta, M.A., Guilherme, L.R.G., Gomez Cuevas, A., Cornejo, L., Cumbal, L., Toujaguez, R., 2012. One century of arsenic exposure in Latin America: A review of history and occurrence from 14 countries. Sci. Total Environ. 429, 2–35.

Bundschuh, J., Armienta, M.A., Morales-Simfors, N., Alam, M.A., López, D.L., Delgado Quezada, V., Dietrich, S., Schneider, J., Joseline Tapia, J., Sracek, O., Castillo, E., Marco Parra, L.-M., Altamirano Espinoza, M., Luiz Roberto Guimarães Guilherme, L. R.G., Sosa, N.N., Niazi, N.K., Tomaszewska, B., Lizama Allende, K., Bieger, K., Alonso, D.L., Brandão, P.F.B., Bhattacharya, P., Litter, M.I., Ahmad, A., 2020. Arsenic in Latin America: New findings on source, mobilization and mobility in human environments in 20 countries based on decadal research 2010-2020. Crit. Rev. Environ. Sci. Technol. https://doi.org/10.1080/10643389.2020.1770527 27.

Cáceres Choque, L.F., Ramos Ramos, O.E., Valdez, S.N., Choque, R.R., Choque, R.G., Fernández, S.G., Sracek, O., Bhattacharya, P., 2013. Fractionation of heavy metals and assessment of contamination of the sediments of Lake Titicaca. Environ. Monit. Assess. J. 185, 9979–9994.

Chilón, E., 1996. Edaphology Manual, First edition. Hisbol Graphic Workshops, La Paz, Bolivia.

Chiron, S., Duwig, C., 2016. Biotic nitrosation of diclofenac in a soil aquifer system (Katari watershed, Bolivia). Sci. Total Environ. 565, 473–480.

Chudnoff, S.M., 2006. A Water Quality Assessment of the Río Katari river and its Principle Tributaries, Bolivia (B.S. Earth and Environmental Science – Geology Option). New Mexico Institute of Mining and Technology, pp. 64–65.

Claesson, M., Fagerberg, J., 2003. 2003. Arsenic in groundwater of Santiago del Estero, Argentina, Department of Land and Water Resources Engineering, KTH, Stock-holm.

CMPRALT (Comisión Multisectorial para la Prevención y Recuperación Ambiental del Lago Titicaca y sus afluentes), 2014. Estado de la calidad ambiental de la cuenca del Lago Titicaca ámbito peruano. D.S. N° 075-2013-PCM.

Coomar, P., Mukherjee, A., Bhattacharya, P., Bundschuh, J., Verma, S., Fryar, A., Ramos Ramos, O., Ormachea Muñoz, M., Gupta, S., Mahanta, C., Quino, I., Thunvik, R., 2019. Contrasting controls on hydrogeochemistry of arsenic-enriched groundwater in the homologous tectonic settings of Andean and Himalayan basin aquifers, Latin America and South Asia. Sci. Total. Environ. 689, 1370–1387.

Davis, C.C., Knocke, W.R., Edwards, M., 2001. Implications of aqueous silica sorption to iron hydroxide: Mobilization of iron colloids and interference with sorption of arsenate and humic substances. Environ. Sci. Technol. 35 (2001), 3158–3162.

Duwig, C., Archundia, D., Lehembre, F., Spadini, L., Morel, M.C., Uzu, G., Chincheros, J., Cortez, R., Martins, J.M.F., 2014. Impacts of anthropogenic activities on the contamination of a sub watershed of Lake Titicaca. Are antibiotics a concern in the Bolivian Altiplano? Proc. Earth Planet. Sci. 10, 370–375.

Espinoza, G., Carvajal, G., Briancon, M., 2016. Determinación de arsénico y otros parámetros en aguas subterráneas en la sub cuenca Titicaca (época de lluvias) (Parte II). Revista de Ingeniería Sanitaria y Ambiental, UMSA, N°3. Facultad de Ingeniería N° 3--2016; La Paz, 2016.

Esri (Environmental Systems Research Institute, Inc.)., 2016. ArcGIS Desktop. How Kriging works. Link: http://desktop.arcgis.com/es/arcmap/10.3/tools/3d-analyst-toolbox/how-kriging-works.htm.

Esri (Environmental Systems Research Institute, Inc.), 2008. ArcGIS Desktop: http://webhelp.esri.com/arcgisdesktop/9.2/index.cfm?TopicName=Classification_methods.

Farnham, I., Singh, A., Stetzenbach, K., Johannesson, K., 2002. Treatment of nondetects in multivariate analysis of groundwater geochemistry data. Chemometrics Intell. Lab. Syst. 60, 265–281.

Filgueiras, A.V., Lavilla, I., Bendicho, C., 2002. Chemical sequential extraction for metal Partitioning in environmental solid samples. J. Environ. Monit. 4, 823–857.

Gleyzes, C., Tellier, S.M., Astruc, M., 2002. Fractionation studies of trace elements in Contaminated soils and Sediments: a review of sequential extraction procedure. Trend Anal. Chem. 21, 451–467.

Google Earth Pro, 2019. Elevation Profile (Cuenca Katari Bajo). Google Earth Pro.

Gustafsson, J.P., Jacks, G., Simonsson, M., Nilsson, I., 2006. Mark-och vattenkemi Teori. Department of Land and Water Resources Engineering, KTH, Stockholm.

Hall, A.H., 2002. Chronic arsenic poisoning. Toxicol. Lett. 128, 69–72.

Hamidian, A., Razeghi, N., Zhang, Y., Yang., M., 2019. Spatial distribution of arsenic in groundwater of Iran, a review. J. Geochem. Explor. https://doi.org/10.1016/j.gexplo.2019.03.014.

Hermansson, E., Karlsson, L., 2004. Occurrence and Distribution of Heavy Metals in the Groundwater of Poopó Basin. Lund University, Sweden, Bolivian Altiplano.

IIS (Instituto de Ingeniería Sanitaria y Ambiental), 2013. Valoración de metales pesados en la cuenca del río Katari y su impacto en la calidad de vida del área de influencia. Proyecto IDH – UMSA "Valoración de metales pesados en la cuenca del Río Katari y su impacto en la calidad de vida del área de influencia". La Paz - Bolivia, 2013.

Instituto Nacional de Estadística (INE), 2017. Census 2012.

Islam, A.B.M.R., Maity, J.P., Bundschuh, J., Chen, C.Y., Bhowmik, B.K., Tazaki, K., 2013. Arsenic mineral dissolution and possible mobilization in mineral-microbe-groundwater environment. J. Hazard. Mater. 262, 989–996.

Jia, Y.F., Guo, H.M., Jiang, Y.X., et al., 2014. Hydrogeochemical zonation and its implication for arsenic mobilization in deep groundwaters near alluvial fans in the Hetao Basin, Inner Mongolia. J. Hydrol. 518, 410–420.

Kapaj, S., Peterson, H., Liber, K., Bhattacharya, P., 2006. Human health effects from chronic arsenic poisoning – A Review. J. Environ. Sci. Health, Part A. 41 (10), 2399–2428. https://doi.org/10.1080/10934520600873571.

Laboratoire d'Hydrogéologie d'Avignon, Université d'Avignon, 1999. Diagrammes software 6.59.

Litter, M.I., Ingallinella, A.M., Olmos, V., Savio, M., Difeo, G., Botto, L., FarfánTorres, E. M., Taylor, S., Frangie, S., Herkovits, J., Schalamuk, I., González, M.J., Berardozzi, E., García Einschlag, F.S., Bhattacharya, P., Ahmad, A., 2019a. Arsenic in Argentina: Occurrence, human health, legislation and determination. Sci. Total Environ. 676, 756–766. https://doi.org/10.1016/j.scitotenv.2019.04.262.

Litter, M.I., Ingallinella, A.M., Olmos, V., Savio, M., Difeo, G., Botto, L., FarfánTorres, E. M., Taylor, S., Frangie, S., Herkovits, J., Schalamuk, I., González, M.J., Berardozzi, E., García Einschlag, F.S., Bhattacharya, P., Ahmad, A., 2019b. Arsenic in Argentina: technologies for arsenic removal from groundwater sources, investment costs and waste management practices. Sci. Total Environ. 690, 778–789. https://doi.org/10.1016/j.scitotenv.2019.06.358.

Maity, J.P., Chen, C.Y., Bundschuh, J., Bhattacharya, P., Mukherjee, A., Chang, Y.F., 2017. Hydrogeochemical reconnaissance of arsenic cycling and possible environmental risk in hydrothermal systems of Taiwan. Groundwater Sustainable Dev. 5, 1–13.

Maity, J.P., Ho, P.R., Huang, Y.H., Sun, A.C., Chen, C.C., Chen, C.Y., 2019. The removal of arsenic from arsenic-bearing groundwater in In-situ and Ex-situ environment using novel natural magnetic rock material and synthesized magnetic material as adsorbent: A comparative assessment. Environ Pollut. 253, 768–778.

Maity, J.P., Kar, S., Liu, J.-H., Jean, J.-S., Chen, C.-Y., Bundschuh, J., Santra, S.C., Liu, C. C., 2011a. The potential for reductive mobilization of arsenic [As(V) to As(III)] by OSBH2 (*Pseudomonas stutzeri*) and OSBH5 (*Bacillus cereus*) in an oil-contaminated site. J. Environ. Sci. Health. Part A Toxic/Hazard. Subst. Environ. Eng. 46 (11), 1239–1246.

Maity, J.P., Nath, B., Chen, C.-Y., Bhattacharya, P., Sracek, O., Bundschuh, J., Kar, S., Thunvik, R., Chatterjee, D., Mukherjee, A.B., Jean, J.S., 2011b. Arsenic-enriched groundwaters of India, Bangladesh and Taiwan–comparison of hydrochemical characteristics and mobility constraints. J. Environ. Sci. Health. Part A Toxic/Hazard. Subst. Environ. Eng. 46 (11), 1163–1176.

Maity, J.P., Nath, B., Kar, S., Chen, C.Y., Banerjee, S., Jean, J.S., Liu, M.Y., Centeno, J.A., Bhattacharya, P., Chang, C.L., Santra, S.C., 2012. Arsenic induced health crisis in peri-urban Moyna and Ardebok villages, West Bengal, India: An exposure assessment study. Environ. Geochem. Health 34 (5), 563–574.

Martínez, I., Zuleta, R., Pacheco, A., Sanjines, J., 2007. International Cooperation on the Lake Titicaca. UNESCO. IHP. WWAP. Technical Documents in Hydrology no. 32, Paris, France.

Mäkelä M., Pöykiö R., Watkins G., Nurmesniemi H. y Dahl O., 2011. Application of a Modified BCR Approach to Investigate the Mobility and Availability of Trace Elements (As, Ba, Cd, Co, Cr, Cu, Mo, Ni, Pb, Zn, and Hg) from a Solid Residue Matrix Designed for Soil Amendment, World Acad. Sci. Eng. Technol. 79.

Mariño, E.E., Teijó Ávila, G., Bhattacharya, P., Schulz, C.J., 2020. The occurrence of arsenic and other trace elements in groundwaters of the southwestern Chaco-Pampean plain, Argentina. J. South Am. Earth Sci. 100, 102547 https://doi.org/10.1016/j.jsames.2020.102547.

McKean, S., 1993. Manual of soil and plant tissue analysis (theoretical and practical guide of methodologies). International Center for Tropical Agriculture - CIAT, Work document number, p. 129.

Meng, X., Korfiatis, G.P., Christodoulatos, C., Bang, S., 2001. Treatment of arsenic in Bangladesh well water using a household co-precipitation and filtration system. Water Res. 35 (12), 2805–2810.

MMAyA (Ministerio de Medio Ambiente y Agua)., 2010. Plan Director de la Cuenca Katari. La Paz, Bolivia.

Mukherjee, A., Bhattacharya, P., Shi, F., Fryar, A.E., Mukherjee, A.B., Xie, Z.M., Sracek, O., Jacks, G., Bundschuh, J., 2009. Trends of solute chemistry evolution in the groundwater of arsenic-affected Huhhot basin, InnerMongolia, P.R. China: its similarity and dissimilarity with the western Bengal basin, India. Appl. Geochem. 24 (12), 1835–1851. https://doi.org/10.1016/j.apgeochem.2009.06.005.

Mukherjee, A., Fryar, A.E., Scanlon, B., Bhattacharya, P., Bhattacharya, A., 2011. Elevated arsenic in deeper groundwater of the western Bengal basin, India: Extent and controls from regional to local scale. Appl. Geochem. 26 (2011), 600–613.

Mukherjee, Abhijit, Sarkar, Soumyajit, Chakraborty, Madhumita, Duttagupta, Srimanti, Bhattacharya, Animesh, Saha, Dipankar, Bhattacharya, Prosun, Mitra, Adway, Gupta, Saibal, 2020. Occurrence, predictors and hazards of elevated groundwater arsenic across India through field observations and regional-scale AI-based modeling. Sci. Total Environ., 143511 https://doi.org/10.1016/j.scitotenv.2020.143511. In press.

Mukherjee, A., Verma, S., Gupta, S., Henke, K.R., Bhattacharya, P., 2014. Influence of tectonics, sedimentation and aqueous flow cycles on the origin of global groundwater origin: Paradigms from three continents. J. Hydrol. 518, 284–299.

Nielsen, D.M., 1991. Practical handbook of ground-water monitoring. Lewis Publishers, US, p. 717.

Nriagu, J.O., Bhattacharya, P., Mukherjee, A.B., Bundschuh, J., Zevenhoven, R., Loeppert, R.H., 2007. Arsenic in soil and groundwater: an overview. In: Bhattacharya, P., Mukherjee, A.B., Bundschuh, J., Zevenhoven, R., Loeppert, R.H. (Eds.), Arsenic in Soil and Groundwater Environment: Biogeochemical Interactions, Health Effects and Remediation, Trace Metals and other Contaminants in the Environment, Volume 9. Elsevier B.V, Amsterdam, The Netherlands, pp. 3–60. https://doi.org/10.1016/S1875-1121(06)09001-8.

Ormachea Muñoz, M., Wern, H., Johnsson, F., Bhattacharya, P., Sracek, O., Thunvik, R., Quintanilla, J., Bundschuh, J., 2013. Geogenic arsenic and other trace elements in the shallow hydrogeologic system of Southern Poopó Basin, Bolivian Altiplano. J. Hazard. Mater. 262, 924–940. https://doi.org/10.1016/j.jhazmat.2013.06.078.

Ormachea Muñoz, M., Garcia Aróstegui, J., Bhattacharya, P., Sracek, O., Garcia Moreno, M., Kohfahl, C., Quintanilla, J., Hornero Diaz, J., Bundschuh, J., 2016. Geochemistry of naturally occurring arsenic in groundwater and surface-water in the southern part of the Poopó Lake basin, Bolivian Altiplano. Groundwater Sustainable Dev. 2–3, 104–116.

ORSTOM, 1991. lnstitut Francais de recherche scientifique pour le développement en cooperation. EL LAGO TITICACA Síntesis del Conocimiento Inmunológico Actual.

Panagiotaras, D., Panagopoulos, G., Papoulis, D., Avramidis, P., 2012. Arsenic geochemistry in groundwater system. In: Panagiotaras, D. (Ed.), Geochemistry–Earth's System Processes. InTech, pp. 27–38.

Parkhurst, D.L., Appelo, C.A.J., 1999. A computer program for speciation, batch-reaction, one-dimensional transport, and inverse geochemical calculations. US Geol. Surv. Water Resour. 99–4259.

Pillco, R., Bengtsson, L., Berndtsson, R., Martí-Cardona, B., Satgé, F., Timouk, F., Bonnet, M., Mollericon, L., Gamarra, C., Pasapera, J., 2019. Modelling Lake Titicaca's daily and monthly evaporation. Hydrol. Earth Syst. Sci. 23, 657–668.

PNUMA (United Nations Environment Programme), 2011. Perspectivas del medio ambiente en el sistema hídrico Titicaca-Desaguadero-Poopó-Salar de Coipasa (TDPS). GEO Titicaca.

PNUMA (United Nations Environment Programme), 2008. Perspectivas del Medio Ambiente Urbano: GEO El Alto. Proyecto GEO ciudades.

Proyecto Piloto Oruro (PPO), 1996. Impact of the Mining and Industrial Contamination in Groundwater, (Impacto de la Contaminación Minera e Industrial Sobre Aguas Subterráneas). Ministerio de Desarrollo Sostenible y Medio Ambiente, Secretaria de Medio Ambiente, Swedish Geological AB, La Paz, Bolivia.

Qin, Y., Ma, Y., Zheng, B., Zhang, L., Zhao, Y., 2014. Temporal and spatial variation of arsenic species in the Dahuofang reservoir in northeast China. Environ. Sci. Pollut. Res. DOI 10.1007/s11356-013-1969-2.

Quino, I., Ormachea, M., Ramos, O., Bhattacharya, P., Quispe, R., Quintanilla, J., Sracek, O., 2019. Hydrochemical assessment with respect to arsenic and other trace elements in the Lower Katari Basin, Bolivian Altiplano. Groundwater Sustainable Dev. https://doi.org/10.1016/j.gsd.2018.11.013.

Quino Lima, I., Ramos Ramos, O., Ormachea Muñoz, M., Aguirre Quintanilla, J., Duwig, C., Prakash Maity, J., Sracek, O., Bhattacharya, P., 2020a. Spatial dependency of arsenic, antimony, boron and other trace elements in the shallow groundwater systems of the Lower Katari Basin, Bolivian Altiplano. Sci. Total Environ. https://doi.org/10.1016/j.scitotenv.2020.137505.

Quino Lima, I., Ormachea Muñoz, M., Ramos Ramos, O.E., Quintanilla Aguirre, J., Maity, J.P., Ahmad, A., Bhattacharya, P., 2020b. Hydrogeochemical contrasts in the shallow aquifer systems of the Lower Katari Basin and Southern Poopó Basin, Bolivian Altiplano. J. S. Am. Earth Sci.

Quintanilla, J., Coudrain-Ribsten, A., Martinez, J., Camacho, V., 1995. Hidroquimica de las aguas del Altiplano de Bolivia (Hydrochemistry of the Waters of the Bolivian Altiplano; in Spanish). In: Ribstein, P., Francou, B., Coudrain-Ribsten, A., Mourguiart, P. (Eds.), "Eaux, Glaciers et Changements Climatiques dans les Andes Tropicales" 24/3. Bull, De l' Institut Français d' Études Andines, pp. 461–471.

Ramos Ramos, O.E., Cáceres, L.F., Ormachea, M.R., Bhattacharya, P., Quino, I., Quintanilla, J., Sracek, O., Thunvik, R., Bundschuh, J., García, M., 2012. Sources and behavior of arsenic and trace elements in groundwater and surface water in the Poopó Lake Basin, Bolivian Altiplano. Environ. Earth Sci. 66 (3), 793–807.

Ramos Ramos, O.E., Rötting, T., French, M., Sracek, O., Bundschuh, J., Quintanilla, J., Bhattacharya, P., 2014. Geochemical processes controlling mobilization of arsenic and trace elements in shallow aquifers and surface waters in the Antequera and Poopó mining regions, Bolivian Altiplano. J. Hydrol. 518, 421–433.

Ravenscroft, P., Brammer, H., Richards, K., 2009. Arsenic Pollution: A Global Synthesis. Sussex, John Wiley & Sons Ltd, p. 588.

Raychowdhury, N., Mukherjee, A., Bhattacharya, P., Johannesson, K., Bundschuh, J., Bejarano, G., Nordberg, E., Martin, R.A., Storniolo, A.R., 2014. Provenance and fate of arsenic and other solutes in the Chaco-Pampean Plain of the Andean foreland, Argentina: from perspectives of hydrogeochemical modeling and regional tectonic setting. J. Hydrol. 518, 300–316.

Ribera Arismendi, M.A., 2010. La Bahía de Cohana. Actualización 2009 – 2010. – La Paz: Serie de estudios de caso sobre problemáticas socio ambientales en Bolivia No 1. LIDEMA, p. 78.

Romero, F.M., Armienta, M.A., Carrillo-Chavez, A., 2004. Arsenic sorption by carbonate-rich aquifer material, a control on arsenic mobility at Zimapán, México. Archiv. Environ. Contam. Toxicol. 47 (2004), 1–13.

Salvarredy-Aranguren, M.M., Probst, A., Roulet, M., Isaure, M.-P., 2008. Contamination of surface waters by mining wastes in the Milluni Valley (Cordillera Real, Bolivia): mineralogical and hydrological influences. Appl. Geochem. 23, 1299–1324.

Samal, A.C., Kar, S., Maity, J.P., Santra, S.C., 2013. Arsenicosis and its relationship with nutritional status in two arsenic affected areas of West Bengal, India. J. Asian Earth Sci. 77, 303–310.

Schnoor, J.L., 1996. Environmental Modeling: Fate and Transport of Pollutants in Water, Air and Soil. John Willey & Sons Inc., New York.

Servant-Vildary, S., Mello e Sousa, S.H., 1993. Palaeohydrology of the Quaternary salineLake Ballivian (southern Bolivian Altiplano) based on diatom studies. Int. J. Salt Lake Res. 2, 69–85.

Silveti, A., Murillo, M., Gonzales, E., Mendoza, V., 2013. Political attribute of technology; BCR sequential chemical extraction method for the diagnosis of heavy metal contamination. Revista Latinoamericana el Ambiente y las Ciencias 4 (8), 51–66.

Smedley, P.L., Kinniburgh, D.G., 2002. A review of the source, behavior and distribution of arsenic in natural waters. Appl. Geochem. 17, 517–568.

Sohrabi, N., Kalantari, N., Amiri, V., Saha, N., Berndtsson, R., Bhattacharya, P., Ahmad, A., 2020. A probabilistic-deterministic analysis of human health risk related to the exposure to potentially toxic elements in groundwater of Urmia coastal aquifer (NW of Iran) with a special focus on arsenic speciation and temporal variation. Stochastic Environ. Res. Risk Assess. https://doi.org/10.1007/s00477-020-01934-6. In press.

Stollenwerk, K.G., 2002. Geochemical processes controlling transport of arsenic in groundwater: a review of adsorption. In: Welch, A.H., Stollenwerk, K.G. (Eds.), Arsenic in Ground Water: Geochemistry and Occurrence. Seacaucus, New Jersey, pp. 67–100.

Tapia, J., Audry, S., 2013. Control of early diagenesis processes on trace metal (Cu, Zn, Cd, Pb and U) and metalloid (As, Sb) behaviors in mining- and smelting-impacted lacustrine environments of the Bolivian Altiplano. Appl. Geochem. 31, 60–78. https://doi.org/10.1016/j.apgeochem.2012.12.006.

Tapia, J., Audry, S., Townley, B., Duprey, J.L., 2012. Geochemical background, baseline and origin of contaminants from sediments in the mining-impacted Altiplano and Eastern Cordillera of Oruro, Bolivia. Geochem. Explor. Environ. Anal. 12, 3–20. https://doi.org/10.1144/1467-7873/10-RA-049.

Tapia, J., Murray, J., Ormachea, M., Tirado, N., Nordstrom, D.K., 2019. Origin, distribution, and geochemistry of arsenic in the Altiplano-Puna plateau of Argentian, Bolivia, Chile, and Peru. Sci. Total. Environ. 678, 309–325.

Tapia, J., Schneider, B., Inostroza, M., Álvarez-Amado, F., Luque, J., Aguilera, F., Parra, S., Bravo, M., 2020. Naturally elevated arsenic in the Altiplano-Puna, Chile and the link to recent (Mio-Pliocene to quaternary) volcanic activity, high crustal thicknesses, and geological structures. J. S. Am. Earth Sci. https://doi.org/10.1016/j.jsames.2020.102905.

Ticona, J., 2018. Eh-pH Graficador v18.jtb.

United Nations, 2019. Economic and Social Commission for Western Asia. https://www.unescwa.org/free-aquifer.

Ure, A.M., Quevauviller, P.H., Muntau, H., Griepink, B., 1993. Speciation of heavy metals in soils and sediments, an account of the improvement and harmonization of extraction techniques undertaken under the auspices of the BCR of the commission of the European Communities. Int. J. Environ. Anal. Chem. 51, 135–151.

Van Den Bergh, K., Laing, G., Du Montoya, J.C., Deckere, E.D., Tack, F.M.G., 2010. Arsenic in drinking water wells on the Bolivian high plain: Field monitoring and effect of salinity on removal efficiency of iron-oxides-containing filters. J. Environ. Sci. Health Part A 45, 1741–1749.

Van Genuchten, C.M., Ahmad, A., 2020. Groundwater As Removal by As(III), Fe(II), and Mn(II) Co-Oxidation: Contrasting As Removal Pathways with O2, NaOCl, and KMnO4. Environ. Sci. Technol. 54 (23), 15454–15464.

Further reading

Aller, L., Bennett, T., Hackett, G., Petty, R., Lehr, J., Sedoris, H., Nielsen, D., Denne, J., 1990. Handbook of suggested practice for the design and installation of ground water monitoring wells. National Water Well Association Dublin. OH. US EPA/600/4-89/034, 221 p.